

Unveiling ν secrets with cosmological data: Neutrino masses and mass hierarchy

Sunny Vagnozzi,^{1,*} Elena Giusarma,^{2,3,4,†} Olga Mena,^{5,‡} Katherine Freese,^{1,6} Martina Gerbino,¹ Shirley Ho,^{2,3,4} and Massimiliano Lattanzi^{7,8}

¹*The Oskar Klein Centre for Cosmoparticle Physics, Department of Physics, Stockholm University, SE-106 91 Stockholm, Sweden*

²*McWilliams Center for Cosmology, Department of Physics, Carnegie Mellon University, Pittsburgh, Pennsylvania 15213, USA*

³*Lawrence Berkeley National Laboratory (LBNL), Physics Division, Berkeley, California 94720-8153, USA*

⁴*Berkeley Center for Cosmological Physics, University of California, Berkeley, California 94720, USA*

⁵*Instituto de Física Corpuscular (IFIC), Universidad de Valencia-CSIC, E-46980 Valencia, Spain*

⁶*Michigan Center for Theoretical Physics, Department of Physics, University of Michigan, Ann Arbor, Michigan 48109, USA*

⁷*Dipartimento di Fisica e Scienze della Terra, Università di Ferrara, I-44122 Ferrara, Italy*

⁸*Istituto Nazionale di Fisica Nucleare (INFN), Sezione di Ferrara, I-44122 Ferrara, Italy*

(Received 3 February 2017; published 1 December 2017)

Using some of the latest cosmological data sets publicly available, we derive the strongest bounds in the literature on the sum of the three active neutrino masses, M_ν , within the assumption of a background flat Λ CDM cosmology. In the most conservative scheme, combining Planck cosmic microwave background temperature anisotropies and baryon acoustic oscillations (BAO) data, as well as the up-to-date constraint on the optical depth to reionization (τ), the tightest 95% confidence level upper bound we find is $M_\nu < 0.151$ eV. The addition of Planck high- ℓ polarization data, which, however, might still be contaminated by systematics, further tightens the bound to $M_\nu < 0.118$ eV. A proper model comparison treatment shows that the two aforementioned combinations disfavor the inverted hierarchy at $\sim 64\%$ C.L. and $\sim 71\%$ C.L., respectively. In addition, we compare the constraining power of measurements of the full-shape galaxy power spectrum versus the BAO signature, from the BOSS survey. Even though the latest BOSS full-shape measurements cover a larger volume and benefit from smaller error bars compared to previous similar measurements, the analysis method commonly adopted results in their constraining power still being less powerful than that of the extracted BAO signal. Our work uses only cosmological data; imposing the constraint $M_\nu > 0.06$ eV from oscillations data would raise the quoted upper bounds by $\mathcal{O}(0.1\sigma)$ and would not affect our conclusions.

DOI: [10.1103/PhysRevD.96.123503](https://doi.org/10.1103/PhysRevD.96.123503)

I. INTRODUCTION

The discovery of neutrino oscillations, which resulted in the 2015 Nobel Prize in Physics [1], has robustly established the fact that neutrinos are massive [2–9]. The results from oscillation experiments can therefore be successfully explained assuming that the three neutrino flavor eigenstates (ν_e, ν_μ, ν_τ) are quantum superpositions of three mass eigenstates (ν_1, ν_2 , and ν_3). In analogy to the quark sector, flavor and mass eigenstates are related via a mixing matrix parametrized by three mixing angles (θ_{12}, θ_{13} , and θ_{23}) and a CP -violating phase δ_{CP} .

Global fits [10–14] to oscillation measurements have determined with unprecedented accuracy five mixing parameters, namely, $\sin^2 \theta_{12}$, $\sin^2 \theta_{13}$, and $\sin^2 \theta_{23}$, as well as the

two mass-squared splittings governing the solar and the atmospheric transitions. The solar mass-squared splitting is given by $\Delta m_{21}^2 \equiv m_2^2 - m_1^2 \simeq 7.6 \times 10^{-5}$ eV². Because of matter effects in the Sun, we know that the mass eigenstate with the larger electron neutrino fraction is the one with the smallest mass. We identify the lighter state with “1” and the heavier state (which has a smaller electron neutrino fraction) with “2.” Consequently, the solar mass-squared splitting is positive. The atmospheric mass-squared splitting is instead given by $|\Delta m_{31}^2| \equiv |m_3^2 - m_1^2| \simeq 2.5 \times 10^{-3}$ eV². Since the sign of the largest mass-squared splitting $|\Delta m_{31}^2|$ remains unknown, there are two possibilities for the mass ordering: the normal hierarchy (NH) ($\Delta m_{31}^2 > 0$, with $m_1 < m_2 < m_3$) and the inverted hierarchy (IH) ($\Delta m_{31}^2 < 0$, and $m_3 < m_1 < m_2$). Other unknowns in the neutrino sector are the presence of CP -violation effects (i.e., the value of δ_{CP}), the θ_{23} octant, the Dirac versus Majorana neutrino nature, and, finally, the absolute neutrino mass scale; see Ref. [15] for a recent review on unknowns of the neutrino sector.

* sunny.vagnozzi@fysik.su.se

† egiusarm@andrew.cmu.edu

‡ omena@ific.uv.es

Cosmology can address two out of the above five unknowns: the absolute mass scale and the mass ordering. Through background effects, cosmology is to zeroth order sensitive to the absolute neutrino mass scale, that is, to the quantity

$$M_\nu \equiv m_{\nu_1} + m_{\nu_2} + m_{\nu_3}, \quad (1)$$

where m_{ν_i} denotes the mass of the i th neutrino mass eigenstate. Indeed, the tightest current bounds on the neutrino mass scale come from cosmological probes; see, for instance, Refs. [16–23]. More subtle perturbation effects make cosmology in principle sensitive to the mass hierarchy as well (see, e.g., Refs. [24–29] for comprehensive reviews on the impact of nonzero neutrino masses on cosmology), although not with current data sets.

As light massive particles, relic neutrinos are relativistic in the early Universe and contribute to the radiation energy density. However, when they turn nonrelativistic at late times, their energy density contributes to the total matter density. Thus, relic neutrinos leave a characteristic imprint on cosmological observables, altering both the background evolution and the spectra of matter perturbations and cosmic microwave background (CMB) anisotropies (see Refs. [24–29] as well as the recent Ref. [30] for a detailed review on massive neutrinos in cosmology, in light of both current and future data sets). The effects of massive neutrinos on cosmological observables will be discussed in detail in Sec. III.

Cosmological probes are primarily sensitive to the sum of the three active neutrino masses M_ν . The exact distribution of the total mass among the three mass eigenstates induces subpercent effects on the different cosmological observables, which are below the sensitivities of ongoing and near future experiments [31–35]. As a result, cosmological constraints on M_ν are usually obtained by making the assumption of a fully degenerate mass spectrum, with the three neutrinos sharing the total mass [$m_{\nu_i} = M_\nu/3$, with $i = 1, 2, 3$, which we will later refer to as “3 deg”]; see Eq. (3)]. Strictly speaking, this is a valid approximation as long as the mass of the lightest eigenstate, $m_0 \equiv m_1(m_3)$ in the case of NH (IH), satisfies

$$m_0 \gg |m_i - m_j|, \quad \forall i, j = 1, 2, 3. \quad (2)$$

The approximation might fail in capturing the exact behavior of massive neutrinos when $M_\nu \sim M_{\nu,\min}$, where $M_{\nu,\min} = \sqrt{\Delta m_{21}^2} + \sqrt{\Delta m_{31}^2} \approx 0.06$ eV [$= \sqrt{\Delta m_{31}^2} + \sqrt{\Delta m_{21}^2} + \Delta m_{21}^2 \approx 0.1$ eV] is the minimal mass allowed by oscillation measurements in the NH (IH) scenario [10–14]; see Appendix A for detailed discussions. Furthermore, it has been argued that the ability to reach a robust upper bound on the total neutrino mass below $M_{\nu,\min} = 0.1$ eV would imply having discarded at some statistical significance the inverted hierarchy scenario. In this case, one has to provide a rigorous statistical treatment of the preference for one hierarchy over the other [36–38].

We will be presenting results obtained within the approximation of three massive degenerate neutrinos. That is, we consider the following mass scheme, which we refer to as 3 deg:

$$m_1 = m_2 = m_3 = \frac{M_\nu}{3} \quad (3 \text{ deg}).$$

This approximation has been adopted by the vast majority of works when M_ν is allowed to vary. This includes the Planck Collaboration, which recently obtained $M_\nu < 0.234$ eV at 95% C.L. [39] through a combination of temperature and low- ℓ polarization anisotropy measurements, within the assumption of a flat Λ CDM + M_ν cosmology. Physically speaking, this choice is dictated by the observation that the impact of the NH and IH mass splittings on cosmological data is tiny if one compares the 3 deg approximation to the corresponding NH and IH models with the same value of the total mass M_ν (see Appendix A for further discussions). For the purpose of comparison with previous work, in Appendix B, we briefly discuss other less physical approximations which have been introduced in the recent literature as well as some of the bounds obtained on M_ν within such approximations.

We present the constraints in light of the most recent cosmological data publicly available. In particular, we make use of i) measurements of the temperature and polarization anisotropies of the CMB as reported by the Planck satellite in the 2015 data release; ii) baryon acoustic oscillations (BAO) measurements from the Sloan Digital Sky Survey III (SDSS-III) Baryon Oscillation Spectroscopic Survey (BOSS) data release 11 CMASS and LOWZ samples and from the Six-degree Field Galaxy Survey (6dFGS) and WiggleZ surveys; iii) measurements of the galaxy power spectrum of the CMASS sample from the SDSS-III BOSS data release 12; iv) local measurements of the Hubble parameter (H_0) from the Hubble Space Telescope; v) the latest measurement of the optical depth to reionization (τ) coming from the analysis of the high-frequency channels of the Planck satellite; and vi) cluster counts from the observation of the thermal Sunyaev-Zeldovich (SZ) effect by the Planck satellite.

In addition to providing bounds on M_ν , we also use these bounds to provide a rigorous statistical treatment of the preference for the NH over the IH. We do so by applying the simple but rigorous method proposed in Ref. [36] and evaluate both posterior odds for NH against IH, as well as the C.L. at which current data sets can disfavor the IH.

The paper is organized as follows. In Sec. II, we describe our analysis methodology. In Sec. III, we instead provide a careful description of the data sets employed, complemented with a full explanation of the physical effects of massive neutrinos on each of them. We showcase our main results in Sec. IV, with Sec. IVA in particular devoted to an analysis of the relative constraining power of the shape power spectrum versus geometrical BAO measurements, whereas

in Sec. IV B, we provide a rigorous quantification of the exclusion limits on the inverted hierarchy from current data sets. Finally, we draw our conclusions in Sec. V.

For the reader who wants to skip to the results, the most important results of this paper can be found in Tables VI, VII, and VIII. The first two of these tables present the most constraining 95% C.L. bounds on the sum of the neutrino masses using a combination of CMB (temperature and polarization), BAO, and other external data sets. The bounds in Table VII have been obtained using also small-scale CMB polarization data, which may be contaminated by systematics, yet we present the results as they are useful for comparing to previous work. Finally, Table VIII presents exclusion limits on the inverted hierarchy neutrino mass ordering, which is disfavored at about 70% C.L. statistical significance.

II. ANALYSIS METHOD

In the following, we shall provide a careful description of the statistical methods employed in order to obtain the bounds on the sum of the three active neutrino masses we show in Sec. IV, as well as caveats to our analyses. Furthermore, we provide a brief description of the statistical method adopted to quantify the exclusion limits on the IH from our bounds on M_ν . For more details on the latter, we refer the reader to Ref. [36] where this method was originally described.

A. Bounds on the total neutrino mass

In our work, we perform standard Bayesian inference (see, e.g., Refs. [40,41] for recent reviews) to derive constraints on the sum of the three active neutrino masses. That is, given a model described by the parameter vector θ and a set of data \mathbf{x} , we derive posterior probabilities of the parameters given the data, $p(\theta|\mathbf{x})$, according to

$$p(\theta|\mathbf{x}) \propto \mathcal{L}(\mathbf{x}|\theta)p(\theta), \quad (3)$$

where $\mathcal{L}(\mathbf{x}|\theta)$ is the likelihood function of the data given the model parameters and $p(\theta)$ denotes the data-independent prior. We derive the posteriors using the Markov chain Monte Carlo (MCMC) sampler COSMOMC with an efficient sampling method [42,43]. To assess the convergence of the generated chains, we employ the Gelman and Rubin statistics [44] $R - 1$, which we require to satisfy $R - 1 < 0.01$ when the data sets do not include SZ cluster counts and $R - 1 < 0.03$ otherwise (this choice is dictated by time and resource considerations: runs involving SZ cluster counts are more computationally expensive than those that do not include SZ clusters, to achieve the same convergence). In this way, the

contribution from statistical fluctuations is roughly a few percent of the limits quoted.¹

We work under the assumption of a background flat Λ CDM Universe and thus consider the following seven-dimensional parameter vector:

$$\theta \equiv \{\Omega_b h^2, \Omega_c h^2, \Theta_s, \tau, n_s, \log(10^{10} A_s), M_\nu\}. \quad (4)$$

Here, $\Omega_b h^2$ and $\Omega_c h^2$ denote the physical baryon and dark matter energy densities, respectively; Θ_s is the ratio of the sound horizon to the angular diameter distance at decoupling; τ indicates the optical depth to reionization; and the details of the primordial density fluctuations are encoded in the amplitude (A_s) and the spectral index (n_s) of its power spectrum at the pivot scale $k_* = 0.05 h \text{ Mpc}^{-1}$. Finally, the sum of the three neutrino masses is denoted by M_ν . For all these parameters, a uniform prior is assumed unless otherwise specified.

Concerning M_ν , we impose the requirement $M_\nu \geq 0$. Thus, we ignore prior information from oscillation experiments, which, as previously stated, set a lower limit of $M_{\nu, \text{min}} \sim 0.06 \text{ eV}$ (0.10 eV) for the NH (IH) mass ordering. If we instead had chosen not to ignore prior information from oscillation experiments, the result would be a slight shift of the center of mass of our posteriors on M_ν toward higher values. As a consequence of these shifts, the 95% C.L. upper limits we report would also be shifted to slightly higher values. Nonetheless, in this way, we can obtain an independent upper limit on M_ν from cosmology alone, while at the same time making the least amount of assumptions. It also allows us to remain open to the possibility of cosmological models predicting a vanishing neutrino density today or models in which the effect of neutrino masses on cosmological observables is hidden due to degeneracies with other parameters (see, e.g., Refs. [46,47]). One can get a feeling for the size of the shifts by comparing our results to those of Ref. [19], in which a prior $M_\nu \geq 0.06 \text{ eV}$ was assumed. As we see, the size of the shifts is small, of $\mathcal{O}(0.1\sigma)$. We summarize the priors on cosmological parameters, as well as some of the main nuisance parameters, in Table I.

All the bounds on M_ν reported in Sec. IV are 95% C.L. upper limits. These bounds depend more or less strongly on our assumption of a background flat Λ CDM model and would differ if one were to consider extended parameter models, for instance scenarios in which the number of relativistic degrees of freedom N_{eff} and/or the dark energy equation of state w are allowed to vary, or if the assumption of flatness is relaxed, and so on. For recent related studies considering extensions to the minimal Λ CDM model, we

¹Notice that this is a very conservative requirement, as a convergence of 0.05 is typically more than sufficient for the exploration of the posterior of a parameter of which the distribution is unimodal [45].

TABLE I. Priors on cosmological and nuisance parameters considered in this work. Priors on a parameter p of the form $[A, B]$ are uniform within the range $A < p < B$, whereas priors of the form $A \pm B$ are Gaussian with central value and variance given by A and B , respectively. The first seven rows refer to the basic parameter vector in Eq. (4). H_0 refers to the Hubble parameter and is a derived parameter, whereas $1 - b$ is the cluster mass bias parameter; see Sec. III F. The parameters b_{HF} and P_{HF} are nuisance parameters used to model the galaxy power spectrum; see Eq. (12).

Parameter	Prior	Name
$\Omega_b h^2$	[0.005,0.1]	...
$\Omega_c h^2$	[0.01,0.99]	...
Θ_s	[0.5,10]	...
τ	[0.01,0.8]	...
	0.055 ± 0.009	$\tau 0p055$
n_s	[0.8,1.2]	...
$\log(10^{10} A_s)$	[2,4]	...
M_ν (eV)	[0,3]	...
H_0 (km/s/Mpc)	[20,100]	(Implicit)
	72.5 ± 2.5	$H072p5$
	73.02 ± 1.79	$H073p02$
$1 - b$	[0.1,1.3]	...
b_{HF}	[0,10]	...
P_{HF}	[0,10000]	...

refer the reader to, e.g., Refs. [47–78] as well as Sec. IV C. For other recent studies which investigate the effect of systematics or the use of data sets not considered here (e.g., cross-correlations between CMB and large-scale structure), see, e.g., Refs. [79,80].

B. Model comparison between mass hierarchies

As we discussed previously, several works have argued that reaching an upper bound on M_ν of order 0.1 eV would imply having discarded the IH at some statistical significance. To quantify the exclusion limits on the IH, a proper model comparison treatment, thus rigorously taking into account volume effects, is required. Various methods which allow the estimation of the exclusion limits on the IH have been devised in the recent literature; see, e.g., Refs. [36–38]. Here, we will briefly describe the simple but rigorous model comparison method, which we will use in our work, proposed by Hannestad and Schwetz in Ref. [36] and based on previous work in Ref. [81]. The method allows the quantification of the statistical significance at which the IH can be discarded, given the cosmological bounds on M_ν . We refer the reader to the original paper [36] for further details.

Let us again consider the likelihood function \mathcal{L} of the data \mathbf{x} given a set of cosmological parameters $\boldsymbol{\theta}$, the mass of the lightest neutrino $m_0 = m_1(m_3)$ for NH (IH), and the discrete parameter H representing the mass hierarchy, with $H = N(I)$ for NH (IH): $\mathcal{L}(\mathbf{x}|\boldsymbol{\theta}, m_0, H)$. Then, given the prior(s) on cosmological parameters $p(\boldsymbol{\theta})$, we define the

likelihood marginalized over cosmological parameters $\boldsymbol{\theta}$ assuming a mass hierarchy H , $\mathcal{E}_H(m_0)$, as

$$\mathcal{E}_H(m_0) \equiv \int d\boldsymbol{\theta} \mathcal{L}(\mathbf{x}|\boldsymbol{\theta}, m_0, H) p(\boldsymbol{\theta}) = \mathcal{L}(\mathbf{x}|m_0, H). \quad (5)$$

Imposing a uniform prior $m_0 \geq 0$ eV and assuming factorizable priors for the other cosmological parameters, it is not hard to show that, as a consequence of Bayes's theorem, the posterior probability of a mass hierarchy H given the data \mathbf{x} , $p_H \equiv p(H|\mathbf{x})$, can be obtained as

$$p_H = \frac{p(H) \int_0^\infty dm_0 \mathcal{E}_H(m_0)}{p(N) \int_0^\infty dm_0 \mathcal{E}_N(m_0) + p(I) \int_0^\infty dm_0 \mathcal{E}_I(m_0)}, \quad (6)$$

where $p(N)$ and $p(I)$ denote priors on the NH and IH, respectively, with $p(N) + p(I) = 1$. The posterior odds of NH against IH are then given by p_N/p_I , whereas the C.L. at which the IH is disfavored, which we refer to as CL_{IH} , is given by

$$\text{CL}_{\text{IH}} = 1 - p_I. \quad (7)$$

The expression in Eq. (6) is correct as long as the assumed prior on m_0 is uniform, and the priors on the other cosmological parameters are factorizable. Different choices of priors on m_0 will of course lead to a larger or smaller preference for the NH. As an example, Ref. [82] considered the effect of logarithmic priors, showing that this leads to a strong preference for the NH (see, however, Ref. [83]).

Another valid possibility, which has not explicitly been considered in the recent literature, is that of performing a model comparison between the two neutrino hierarchies by imposing a uniform prior on M_ν instead of m_0 . In this case, it is easy to show that the posterior odds for NH against IH, p_N/p_I , is given by (considering for simplicity the case in which NH and IH are assigned equal priors)

$$\frac{p_N}{p_I} \equiv \frac{\int_{0.06 \text{ eV}}^\infty dM_\nu \mathcal{E}(M_\nu)}{\int_{0.10 \text{ eV}}^\infty dM_\nu \mathcal{E}(M_\nu)}, \quad (8)$$

where, analogously to Eq. (5), we define the marginal likelihood $\mathcal{E}(M_\nu)$ as

$$\mathcal{E}_H(M_\nu) \equiv \int d\boldsymbol{\theta} \mathcal{L}(\mathbf{x}|\boldsymbol{\theta}, M_\nu, H) p(\boldsymbol{\theta}) = \mathcal{L}(\mathbf{x}|M_\nu, H). \quad (9)$$

It is actually easy to show that in the low-mass region of parameter space currently favored by cosmological data, i.e., $M_\nu \lesssim 0.15$ eV, the posterior odds for NH against IH one obtains by choosing a flat prior on M_ν [Eq. (8)] or a flat prior on m_0 [Eq. (6)] are to very good approximation equal. It is also interesting to note that, as is easily seen from Eq. (8), cosmological data will always prefer the normal hierarchy over the inverted hierarchy, simply as a consequence of volume effects; that is, the volume of parameter space available to the normal hierarchy ($M_\nu > 0.06$ eV) is greater than that available to the inverted hierarchy

($M_\nu > 0.1$ eV). For this reason, the way the prior volume is weighted plays a crucial role in determining the preference for one hierarchy over the other (see discussions in Refs. [82,83]).

In our work, we choose to follow the prescription of Ref. [36] (based on a uniform prior on m_0) and hence apply Eq. (6) to determine the preference for the normal hierarchy over the inverted one from cosmological data.

III. DATA SETS AND THEIR SENSITIVITY TO M_ν

We present below a detailed description of the data sets used in our analyses and their modeling, discussing their sensitivity to the sum of the active neutrino masses. For clarity, all the denominations of the combinations of data sets we consider are summarized in Table II. For plots comparing cosmological observables in the presence or absence of massive neutrinos, we refer the reader to Refs. [24–29] and especially Fig. 1 of the recent Ref. [30].

A. Cosmic microwave background

Neutrinos leave an imprint on the CMB (both at the background and at the perturbation level) in, at least, five different ways, extensively explored in the literature [24–30]:

- (i) By delaying the epoch of matter-radiation equality, massive neutrinos lead to an enhanced early integrated Sachs-Wolfe (EISW) effect [28]. This effect is due to the time variation of gravitational potentials, which occurs during the radiation-dominated era, but not during the matter-dominated era, and leads to an enhancement of the first acoustic peak in particular. Traditionally, this has been the most relevant neutrino mass signature as far as CMB data are concerned.
- (ii) Because of the same delay as above, light ($f_\nu < 0.1$) massive neutrinos actually increase the comoving

TABLE II. Specific data sets and combinations thereof used in this work and associated references of work in which the data are presented and/or discussed.

Data set	Content	References
<i>base</i>	<i>PlanckTT + lowP</i>	[39,84]
<i>basepol</i>	<i>PlanckTT + lowP + highP</i>	[39,84]
<i>P(k)</i>	SDSS-III BOSS DR12 CMASS <i>P(k)</i>	[85]
<i>BAO</i>	BAO from 6dFGS BAO, WiggleZ, SDSS-III BOSS DR11 LOWZ	[86–88]
<i>BAOFULL</i>	BAO from 6dFGS, WiggleZ, SDSS-III BOSS DR11 LOWZ, SDSS-III BOSS DR11 CMASS	[86–88]
<i>basePK</i>	<i>base + P(k) + BAO</i>	[39,84–88]
<i>basepolPK</i>	<i>basepol + P(k) + BAO</i>	[39,84–88]
<i>baseBAO</i>	<i>base + BAOFULL</i>	[39,84–88]
<i>basepolBAO</i>	<i>basepol + BAOFULL</i>	[39,84–88]
<i>SZ</i>	Planck SZ clusters	[89,90]

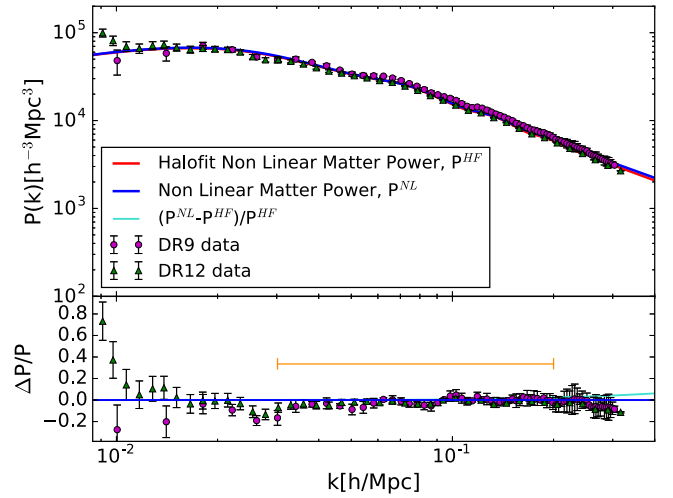


FIG. 1. *Top*: Nonlinear galaxy power spectrum computed using the HALOFIT method with the CAMB code [124] (red line) and the Coyote emulator (blue line) [120–122] at $z = 0.57$ for the Λ CDM best-fit parameters from *Planck TT* 2015 data and $M_\nu = 0$ eV (given that the emulator does not fully implement corrections due to nonzero neutrino masses on small scales). Green triangle data points are the clustering measurements from the BOSS DR12 CMASS sample. The error bars are computed from the diagonal elements C_{ii} of the covariance matrix. For comparison with previous work [23], purple circles represent clustering measurements from the BOSS DR9 CMASS sample. A very slight suppression in power on small scales (large k) of the DR12 sample compared to the DR9 sample is visible. Note that the binning strategies adopted in DR9 and DR12 are different. *Bottom*: Residuals with respect to the nonlinear model with HALOFIT. The orange horizontal line indicates the k range used in our analysis. As is visually clear, the k range we choose is safe from large nonlinear corrections.

sound horizon at decoupling $r_s(z_{\text{dec}})$, thus increasing the angular size of the sound horizon at decoupling Θ_s and shifting all the peaks to lower multipoles ℓ 's [24].

- (ii) By suppressing the structure growth on small scales due to their large thermal velocities (see further details later in Sec. III B), massive neutrinos reduce the lensing potential and hence the smearing of the high- ℓ multipoles due to gravitational lensing [91]. This is a promising route toward determining both the absolute neutrino mass scale and the neutrino mass hierarchy (see, e.g., Refs. [92,93]) because it probes the matter distribution in the linear regime at higher redshift and because the unlensed background is precisely understood. CMB lensing suffers from systematics as well, although these tend to be of instrumental origin and hence decrease with higher resolution. In fact, a combination of CMB-S4 [94–96] lensing and DESI [97–99] BAO is expected to achieve an uncertainty on M_ν of 0.016 eV [94].
- (iv) Massive neutrinos will also lead to a small change in the diffusion scale, which affects the photon

diffusion pattern at high- ℓ multipoles [28], although again this effect is important only for neutrinos which are nonrelativistic at decoupling, i.e., for $M_\nu > 0.6$ eV.

- (v) Finally, since the enhancement of the first peak due to the EISW depends, in principle, on the precise epoch of transition to the nonrelativistic regime of each neutrino species, that is, on the individual neutrino masses, future CMB-only measurements such as those of Refs. [94–96,100–109] could, although only in a very optimistic scenario, provide some hints to unravel the neutrino mass ordering [28]. Current data instead have no sensitivity to this effect.²

Although all the above effects may suggest that the CMB is exquisitely sensitive to the neutrino mass, in practice, the shape of the CMB anisotropy spectra is governed by several parameters, some of which are degenerate among themselves [110,111]. We refer the reader to the dedicated study of Ref. [30] (see also Ref. [112]).

To assess the impact of massive neutrinos on the CMB, all characteristic times, scales, and density ratios governing the shape of the CMB anisotropy spectrum should be kept fixed, i.e., keeping z_{eq} and the angular diameter distance to last scattering $d_A(z_{\text{dec}})$ fixed. This would result in a decrease in the late integrated Sachs-Wolfe (LISW) effect, which, however, is poorly constrained owing to the fact that the relevant multipole range is cosmic variance limited; a modest change in the diffusion damping scale for $M_\nu \gtrsim 0.6$ eV; and, finally, a $\Delta C_\ell/C_\ell \sim -(M_\nu/0.1 \text{ eV})\%$ depletion of the amplitude of the C_ℓ 's for $20 \lesssim \ell \lesssim 200$, due to a smaller EISW effect, which also contains a sub-permil effect due to the individual neutrino masses, essentially impossible to detect.

1. Baseline combinations of data sets used and their definitions, I

Measurements of the CMB temperature, polarization, and cross-correlation spectra from the Planck 2015 data release [39,113] are included. We consider a combination of the high- ℓ ($30 \leq \ell \leq 2508$) TT likelihood, as well as the low- ℓ ($2 \leq \ell \leq 29$) TT likelihood based on the CMB maps recovered with COMMANDER; we refer to this combination as *PlanckTT*. We furthermore include the Planck polarization data in the low- ℓ ($2 \leq \ell \leq 29$) likelihood, referring to it as *lowP*. Our baseline model, consisting of a combination of *PlanckTT* and *lowP*, is referred to as *base*.

²The effect is below the $\%$ level for all multipoles, hence well beyond the reach of Planck. The effect will be below the reach of ground-based Stage-III experiments such as Advanced ACTPol [100,101], SPT-3G [102], the Simons Array [103], and the Simons Observatory [104]. It will most likely be below the reach of ground-based Stage-IV experiments such as CMB-S4 [94–96] or next-generation satellites such as the proposed LiteBIRD [105], CoRE [106,107], and PIXIE [109].

In addition to the above, we also consider the high- ℓ ($30 \leq \ell \leq 1996$) EE and TE likelihood, which we refer to as *highP*. To ease the comparison of our results to those previously presented in the literature, we shall add high- ℓ polarization measurements to our baseline model separately, referring to the combination of *base* and *highP* as *basepol*. For the purpose of clarity, we have summarized our nomenclature of data sets and their combinations in Table II.

All the measurements described above are analyzed by means of the publicly available Planck likelihoods [84].³ When considering a prior on the optical depth to reionization τ , we shall only consider the TT likelihood in the multipole range $2 \leq \ell \leq 29$. We do so to avoid double-counting of information; see Sec. III E. Of course, these likelihoods depend also on a number of nuisance parameters, which should be (and are) marginalized over. These nuisance parameters describe, for instance, residual foreground contamination, calibration, and beam leakage (see Refs. [39,84]).

CMB measurements have been complemented with additional probes, which will help break the parameter degeneracies discussed. These additional data sets include large-scale structure probes and direct measurements of the Hubble parameter and will be described in what follows. We make the conservative choice of not including lensing potential measurements, despite that measuring M_ν via lensing potential reconstruction is the expected target of the next-generation CMB experiments. This choice is dictated by the observation that lensing potential measurements via reconstruction through the temperature four-point function are known to be in tension with the lensing amplitude as constrained by the CMB power spectra through the A_{lens} parameter [39] (see also Refs. [114–117] for relevant work).

B. Galaxy power spectrum

Once CMB data are used to fix the other cosmological parameters, the galaxy power spectrum could in principle be the most sensitive cosmological probe of massive neutrinos among those exploited here. Sub-eV neutrinos behave as a hot dark matter component with large thermal velocities, clustering only on scales below the neutrino free-streaming wave number k_{fs} [26,28]:

$$k_{\text{fs}} \simeq 0.018 \Omega_m^{1/2} \left(\frac{M_\nu}{1 \text{ eV}} \right)^{1/2} h \text{ Mpc}^{-1}. \quad (10)$$

On scales below the free-streaming scale (or, correspondingly, for wave numbers larger than the free-streaming wave number), neutrinos cannot cluster as their thermal velocity exceeds the escape velocity of the gravitational potentials on those scales. Conversely, on scales well above the free-streaming scale, neutrinos behave as cold dark

³www.cosmos.esa.int/web/planck/pla.

matter after the transition to the nonrelativistic regime. Massive neutrinos leave their imprint on the galaxy power spectrum in several different ways:

- (i) For wave numbers $k > k_{\text{fs}}$, the power spectrum in the linear perturbation regime is subject to a scale-independent reduction by a factor of $(1 - f_\nu)^2$, where $f_\nu \equiv \Omega_\nu/\Omega_m$ is defined as the ratio of the energy content in neutrinos to that in matter [28].
- (ii) In addition, the power spectrum for wave numbers $k > k_{\text{fs}}$ is further subject to a scale-dependent step-like suppression, starting at k_{fs} and saturating at $k \sim 1 \text{ h Mpc}^{-1}$. This suppression is due to the absence of neutrino perturbations in the total matter power spectrum, ultimately due to the fact that neutrinos do not cluster on scales $k > k_{\text{fs}}$. At $k \sim 1 \text{ h Mpc}^{-1}$, the suppression reaches a constant amplitude of $\Delta P(k)/P(k) \simeq -10f_\nu$ [28] (the amplitude of the suppression is independent of redshift; however, see the point below).
- (iii) The growth rate of the dark matter perturbations is reduced from $\delta \propto a$ to $\delta \propto a^{1-\frac{3}{2}f_\nu}$, due to the absence of gravitational backreaction effects from free-streaming neutrinos. The redshift dependence of this suppression implies that this effect could be disentangled from that of a similar suppression in the primordial power spectrum by measuring the galaxy power spectrum at several redshifts, which amounts to measuring the time dependence of the neutrino mass effect [28].
- (iv) On very large scales ($10^{-3} < k < 10^{-2}$), the matter power spectrum is enhanced by the presence of massive neutrinos [118].
- (v) As in the case of the EISW effect in the CMB, the step-like suppression in the matter power spectrum carries a nontrivial dependence on the individual neutrino masses, as it depends on the time of the transition to the nonrelativistic regime for each neutrino mass eigenstate [31,34] ($k_{\text{fs}} \propto m_{\nu_i}^{1/2}$) and thus is in principle extremely sensitive to the neutrino mass hierarchy. However, the effect is very small and very hard to measure, even with the most ambitious next-generation large-scale structure surveys [32,33,35]. Through the same effect, the lensed CMB as well as the lensing potential power spectrum could also be sensitive to the neutrino mass hierarchy.

Notice that, in principle, once CMB data are used to fix the other cosmological parameters, the galaxy power spectrum could be the most sensitive probe of neutrino masses. In practice, the potential of this data set is limited by several effects. Galaxy surveys have access to a region of k space $k_{\text{min}} < k < k_{\text{max}}$ where the step-like suppression effect is neither null nor maximal. The minimum wave number accessible is limited both by signal-to-noise ratio and by systematics effects and is typically of order $k \sim 10^{-2} \text{ h Mpc}^{-1}$, meaning that the fourth effect outlined above is currently not appreciable. The maximum wave

number accessible is instead limited by the reliability of the nonlinear predictions for the matter power spectrum.

At any given redshift, there exists a nonlinear wave number, above which the galaxy power spectrum is only useful insofar as one is able to model nonlinear effects, redshift space distortions, and the possible scale dependence of the bias (a factor relating the spatial distribution of galaxies and the underlying dark matter density field [119]) correctly. The nonlinear wave number depends not only on the redshift of the sample but also on other characteristics of the sample itself (e.g., whether the galaxies are more or less massive). At the present time, the nonlinear wave number is approximately $k = 0.15 \text{ h Mpc}^{-1}$, whereas for the galaxy sample we will consider [Data Release (DR) 12 CMASS, at an effective redshift of $z = 0.57$; see footnote 4 for the definition of effective redshift], we will show that wave numbers smaller than $k = 0.2 \text{ h Mpc}^{-1}$ are safe against large nonlinear corrections (see also Fig. 1, where the galaxy power spectrum has been evaluated for $M_\nu = 0 \text{ eV}$ given that the Coyote emulator adopted [120–122] does not fully implement corrections due to nonzero neutrino masses on small scales, and Ref. [23]).⁴

The issue of the scale-dependent bias is indeed more subtle than it might seem, given that neutrinos themselves induce a scale-dependent bias [125–127]. A parametrization of the galaxy power spectrum in the presence of massive neutrinos in terms of a scale-independent bias and a shot-noise component [see Eq. (12)], which in itself adds two extra nuisance parameters, may not capture all the relevant effects at play. Despite these difficulties, the galaxy power spectrum is still a very useful data set as it helps break some of the degeneracies present with CMB-only data, in particular by improving the determination of $\Omega_m h^2$ and n_s , the latter being slightly degenerate with M_ν . Moreover, as we shall show in this paper, the galaxy power spectrum represents a conservative data set (see Sec. IV A).

Nonetheless, a great deal of effort is being invested into determining the scale-dependent bias from cosmological data sets. There are several promising routes toward achieving this, for instance, through CMB lensing, galaxy lensing, cross-correlations of the former with galaxy or quasar clustering measurements, or higher-order correlators of the former data sets; see, e.g., Refs. [128–136]. A sensitivity on M_ν of 0.023 eV has been forecasted from a combination of Planck CMB measurements together with weak lensing shear autocorrelation, galaxy autocorrelation, and galaxy-shear cross-correlation from Euclid [137], after marginalization over the bias, with the figure improving to 0.01 eV after including a weak lensing–selected cluster sample from Euclid [137–142]. Similar results are expected to be achieved for certain configurations of the proposed WFIRST survey

⁴The effective redshift consists of the weighted mean redshift of the galaxies of the sample, with the weights described in Ref. [123].

[143]. It is worth considering that the sensitivity of these data sets would be substantially boosted by determining the scale-dependent bias as discussed above.

A conservative cutoff in wave number space, required in order to avoid nonlinearities when dealing with galaxy power spectrum data, denies access to the modes in which the signature of nonzero M_ν is greatest, i.e., those at high k where the free-streaming suppression effect is most evident. One is then brought to question the usefulness of such data when constraining M_ν . Actually, the real power of $P(k)$ rests in its degeneracy breaking ability, when combined with CMB data. For example, $P(k)$ data are extremely useful as far as the determination of certain cosmological parameters is concerned (e.g., n_s , which is degenerate with M_ν).

The degeneracy breaking effect of $P(k)$, however, is most evident when in combination with CMB data. For an example, let us consider what is usually referred to as the most significant effect of nonzero M_ν on $P(k)$, that is, a steplike suppression of the small-scale power spectrum. This effect is clearest when one increases M_ν while fixing (Ω_m, h) . However, as we discussed in Sec. III A, the impact of nonzero M_ν on CMB data is best examined fixing Θ_s . If one adjusts h in order to keep Θ_s fixed, and in addition keeps $\Omega_b h^2$ and $\Omega_c h^2$ fixed, the power spectrum will be suppressed on both large and small scales; i.e., the result will be a global increase in amplitude [144]. In other words, this reverses the fourth effect listed above. This is just an example of the degeneracy breaking power of $P(k)$ data in combination with CMB data.

Galaxy clustering measurements are addressed by means of the SDSS-III [145] BOSS [146–148] DR12 [123,149]. The SDSS-III BOSS DR12CMAS sample covers an effective volume of $V_{\text{eff}} \approx 7.4 \text{ Gpc}^3$ [150]. It contains 777,202 massive galaxies in the range $0.43 < z < 0.7$, at an effective redshift $z = 0.57$ (see footnote 4 for the definition of effective redshift), covering 9376.09 deg^2 over the sky. Here, we consider the spherically averaged power spectrum of this sample, as measured by Gil-Marín *et al.* in Ref. [85]. We refer to this data set as $P(k)$. The measured galaxy power spectrum P_{meas}^g consists of a convolution of the true galaxy power spectrum P_{true}^g with a window function $W(k_i, k_j)$, which accounts for correlations between the measurements at different scales due to the finite size of the survey geometry:

$$P_{\text{meas}}^g(k_i) = \sum_j W(k_i, k_j) P_{\text{true}}^g(k_j) \quad (11)$$

Thus, at each step of the Monte Carlo, we need to convolve the theoretical galaxy power spectrum P_{th} at the given point in the parameter space with the window function, before comparing it with the measured galaxy power spectrum and constructing the likelihood.

Following previous works [151,152], we model the theoretical galaxy power spectrum as

$$P_{\text{th}} = b_{\text{HF}}^2 P_{\text{HF}\nu}^m(k, z) + P_{\text{HF}}^s, \quad (12)$$

where $P_{\text{HF}\nu}^m$ denotes the matter power spectrum calculated at each step by the Boltzmann solver CAMB, corrected for nonlinear effects using the HALOFIT method [153,154]. We make use of the modified version of HALOFIT designed by Ref. [155] to improve the treatment of nonlinearities in the presence of massive neutrinos. To reduce the impact of nonlinearities, we impose the conservative choice of considering a maximum wave number $k_{\text{max}} = 0.2 \text{ h Mpc}^{-1}$. As we show in Fig. 1 (for $M_\nu = 0 \text{ eV}$), this region is safe against uncertainties due to nonlinear evolution and is also convenient for comparison with other works which have adopted a similar maximum wave number cutoff. The smallest wave number we are considering is instead of $k_{\text{min}} = 0.03 \text{ h Mpc}^{-1}$ and is determined by the control over systematics, which dominate at smaller wave numbers. The parameters b_{HF} and P_{HF}^s denote the scale-independent bias and the shot noise contributions; the former reflects the fact that galaxies are biased tracers of the underlying dark matter distribution, whereas the latter arises from the discrete pointlike nature of the galaxies as tracers of the dark matter. We impose flat priors in the range $[0.1, 10]$ and $[0, 10000]$, respectively, for b_{HF} and P_{HF}^s .

Although in this simple model the bias and shot noise are assumed to be scale independent, there is no unique prescription for the form of these quantities. In particular, concerning the bias, several theoretically well-motivated scale-dependent functional forms exist in the literature (such as the Q model of Ref. [156], that of Ref. [157], or that of Ref. [158] motivated by local primordial non-Gaussianity). It is beyond the scope of our paper to explore the impact of different bias function choices on the neutrino mass bounds. Instead, we simply note that it is not necessarily true that increasing the number of parameters governing the bias shape may result in broader constraints. Indeed, tighter constraints on M_ν may arise in some of the bias parametrizations with more than one parameter involved because they might have comparable effects on the power spectrum.

C. Baryon acoustic oscillations

Prior to the recombination epoch, photons and baryons in the early Universe behave as a tightly coupled fluid, the evolution of which is determined by the interplay between the gravitational pull of potential wells and the restoring force due to the large pressure of the radiation component. The resulting pressure waves which set up, before freezing at recombination, imprint a characteristic scale on the late-time matter clustering, in the form of a localized peak in the two-point correlation function or a series of smeared peaks in the power spectrum. This scale corresponds to the sound horizon at the drag epoch, denoted by $r_s(z_{\text{drag}})$, where the drag epoch is defined as the time when baryons were released from the Compton drag of photons; see Ref. [159]. Then, $r_s(z_{\text{drag}})$ takes the form

$$r_s(z_{\text{drag}}) = \int_{z_{\text{drag}}}^{\infty} dz \frac{c_s(z)}{H(z)}, \quad (13)$$

where $c_s(z)$ denotes the sound speed and is given by $c_s(z) = c/\sqrt{3(1+R)}$, with $R = 3\rho_b/4\rho_r$ being the ratio of the baryon to photon momentum density. Finally, the baryon drag epoch z_{drag} is defined as the redshift such that the baryon drag optical depth τ_{drag} is equal to 1,

$$\tau_{\text{drag}}(\eta_{\text{drag}}) = \frac{4\Omega_r}{3\Omega_b} \int_0^{z_{\text{drag}}} dz \frac{d\eta}{da} \frac{\sigma_T x_e(z)}{1+z} = 1, \quad (14)$$

where $\sigma_T = 6.65 \times 10^{-29} \text{ m}^2$ denotes the Thomson cross section and $x_e(z)$ represents the fraction of free electrons.

BAO measurements contain geometrical information in the sense that, as a ‘‘standard ruler’’ of known and measured length, they allow for the determination of the angular diameter distance to the redshift of interest and hence make it possible to map out the expansion history of the Universe after the last scattering. In addition, they are affected by uncertainties due to the nonlinear evolution of the matter density field to a lesser extent than the galaxy power spectrum, making them less prone to systematic effects than the latter. An angle-averaged BAO measurement constrains the quantity $D_v(z_{\text{eff}})/r_s(z_{\text{drag}})$, where the dilation scale D_v at the effective redshift of the survey z_{eff} is a combination of the physical angular diameter distance $D_A(z)$ and the Hubble parameter $H(z)$ (which control the radial and the tangential separations within a given cosmology, respectively):

$$D_v(z) = \left[(1+z)^2 D_A(z)^2 \frac{cz}{H(z)} \right]^{\frac{1}{3}}. \quad (15)$$

D_v quantifies the dilation in distances when the fiducial cosmology is modified. The power of the BAO technique resides on its ability to resolve the existing degeneracies present when the CMB data alone are used, in particular, in sharpening the determination of Ω_m and of the Hubble parameter H_0 , discarding the low values of H_0 allowed by the CMB data.

Massive neutrinos affect both the low-redshift geometry and the growth of structure, and correspondingly BAO measurements. If we increase M_ν , while keeping $\Omega_b h^2$ and $\Omega_c h^2$ fixed, the expansion rate at early times is increased, although only for $M_\nu > 0.6 \text{ eV}$. Therefore, in order to keep fixed the angular scale of the sound horizon at last scattering Θ_s (which is very well constrained by the CMB acoustic peak structure), it is necessary to decrease Ω_Λ . As Ω_Λ decreases, it is found that $H(z)$ decreases for $z < 1$ [160,161]. It can be shown that an increase in M_ν has a negligible effect on $r_s(z_{\text{drag}})$. Hence, we conclude that the main effect of massive neutrinos on BAO measurements is to increase $D_v(z)/r_s(z_{\text{drag}})$ and decrease H_0 , as M_ν is increased (see Ref. [161]). It is worth noting that there is no parameter degeneracy which can cancel the effect of a

nonzero neutrino mass on BAO data alone, as far as the minimal $\Lambda\text{CDM} + M_\nu$ extended model is concerned [30].

1. Baseline combinations of data sets used and their definitions, II

In this work, we make use of BAO measurements extracted from a number of galaxy surveys. When using BAO measurements in combination with the DR12 CMASS $P(k)$, we consider data from the 6dFGS [86], the WiggleZ survey [87], and the DR11 LOWZ sample [88], as is done in Ref. [23]. We refer to the combination of these three BAO measurements as *BAO*. When combining *BAO* with the *base* CMB data set and the DR12 CMASS $P(k)$ measurements, we refer to the combination as *basePK*. When combining *BAO* with the *basepol* CMB data set and the DR12 CMASS $P(k)$ measurements, we refer to the combination as *basepolPK*. Recall that we have summarized our nomenclature of data sets (including baseline data sets) and their combinations in Table II.

The 6dFGS data consist of a measurement of $r_s(z_{\text{drag}})/D_V(z)$ at $z = 0.106$ (as per the discussion above, r_s/D_V decreases as M_ν is increased). The WiggleZ data instead consist of measurements of the acoustic parameter $A(z)$ at three redshifts, $z = 0.44$, $z = 0.6$, and $z = 0.73$, where the acoustic parameter is defined as

$$A(z) = \frac{100D_v(z)\sqrt{\Omega_m h^2}}{cz}. \quad (16)$$

Given the effect of M_ν on $D_v(z)$, $A(z)$ will increase as M_ν increases. Finally, the DR11 LOWZ data consist of a measurement of $D_v(z)/r_s(z_{\text{drag}})$ (which increases as M_ν is increased) at $z = 0.32$.

Since the BAO feature is measured from the galaxy two-point correlation function, to avoid the double-counting of information, when considering the *base* and *basepol* data sets, we do not include the DR11 CMASS BAO measurements, as the DR11CMASS and DR12CMASS volumes overlap. However, if we drop the DR12CMASS power spectrum from our data sets, we are allowed to add DR11CMASS BAO measurements without this leading to the double-counting of information. Therefore, for completeness, we consider this case as well. Namely, we drop the DR12CMASS power spectrum from our data sets, replacing it with the DR11CMASS BAO measurement. This consists of a measurement of $D_v(z_{\text{eff}})/r_s(z_{\text{drag}})$ at $z_{\text{eff}} = 0.57$.

2. Baseline combinations of datasets used and their definitions, III

We refer to the combination of the four BAO measurements (6dFGS, WiggleZ, DR11 LOWZ, and DR11 CMASS) as *BAOFULL*. We instead refer to the combination of the

TABLE III. Baryon acoustic oscillation measurements considered in this work. From left to right, the columns display the survey, the type of measurement, the effective redshift, the measurement, and the associated reference.

Data set	Type of measurement	z_{eff}	Measurement	Reference
6dFGS	$r_s(z_{\text{drag}})/D_v(z_{\text{eff}})$	0.106	0.336 ± 0.015	[86]
WiggleZ	$A(z)$	0.44	0.474 ± 0.034	[87]
	$A(z)$	0.60	0.442 ± 0.020	[87]
	$A(z)$	0.73	0.424 ± 0.021	[87]
BOSS DR11 LOWZ	$D_v(z_{\text{eff}})/r_s(z_{\text{drag}})$	0.32	8.250 ± 0.170	[88]
BOSS DR11 CMASS	$D_v(z_{\text{eff}})/r_s(z_{\text{drag}})$	0.57	13.773 ± 0.134	[88]

base CMB and the *BAOFULL* data sets with the nomenclature *baseBAO*. When high- ℓ polarization CMB data are added to this *baseBAO* data set, the combination is referred to as *basepolBAO*; see Table II. The comparison between *basePK* and *baseBAO*, as well as between *basepolPK* and *basepolBAO*, gives insight into the role played by large-scale structure data sets in constraining neutrino masses. In particular, it allows for an assessment of the relative importance of shape information in the form of the power spectrum against geometrical information in the form of BAO measurements when deriving the neutrino mass bounds. For clarity, all the denominations of the combinations of data sets we consider are summarized in Table II.

All the BAO measurements used in this work are tabulated in Table III. Note that we do not include BAO measurements from the DR7 main galaxy sample [162] or from the cross-correlation of DR11 quasars with the Ly α forest absorption [163], and hence our results are not directly comparable to other existing studies which included these measurements.

D. Hubble parameter measurements

Direct measurements of H_0 are very important when considering bounds on M_ν . With CMB data alone, there exists a strong degeneracy between M_ν and H_0 (see, e.g., Ref. [164]). When M_ν is varied, the distance to last scattering changes as well. Defining $\omega_b \equiv \Omega_b h^2$, $\omega_c \equiv \Omega_c h^2$, $\omega_m \equiv \Omega_m h^2$, $\omega_r \equiv \Omega_r h^2$, and $\omega_\nu \equiv \Omega_\nu h^2$, within a flat Universe, this distance is given by

$$\chi = c \int_0^{z_{\text{dec}}} \frac{dz}{\sqrt{\omega_r(1+z)^4 + \omega_m(1+z)^3 + (1 - \frac{\omega_m}{h^2})}}, \quad (17)$$

where $\omega_m = \omega_c + \omega_b + \omega_\nu$. The structure of the CMB acoustic peaks leaves little freedom in varying ω_c and ω_b . Therefore, for what concerns the distance to the last scattering, a change in M_ν can be compensated essentially only by a change in h or, in other words, by a change in H_0 . This suggests that M_ν and H_0 are strongly anticorrelated; the effect on the CMB of increasing M_ν can be easily compensated by a decrease in H_0 and vice versa.

In light of the above discussion, we expect a prior on the Hubble parameter to help pin down the allowed values of

M_ν from CMB data. Here, we consider two different priors on the Hubble parameter. The first prior we consider is based on a reanalysis of an older measurement based on the Hubble Space Telescope, the original measurement being $H_0 = (73.8 \pm 2.4) \text{ km s}^{-1} \text{ Mpc}^{-1}$ [165]. The original measurement showed a $\sim 2.4\sigma$ tension with the value of H_0 derived from fitting CMB data [39,93]. The reanalysis, conducted by Efstathiou in Ref. [166], used the revised geometric maser distance to NGC4258 of Ref. [167] as a distance anchor. This reanalysis obtains a more conservative value of $H_0 = (70.6 \pm 3.3) \text{ km s}^{-1} \text{ Mpc}^{-1}$, which agrees with the extracted H_0 value from CMB-only data within 1σ . We refer to this prior as *H070p6*.

The second prior we consider is based on the most recent Hubble Space Telescope (HST) 2.4% determination of the Hubble parameter in Ref. [168]. This measurement benefits from more than twice the number of Cepheid variables used to calibrate luminosity distances, with respect to the previous analysis [165], as well as from improved determinations of distance anchors. The measured value of the Hubble parameter is $H_0 = (73.02 \pm 1.79) \text{ km s}^{-1} \text{ Mpc}^{-1}$, which is in tension with the CMB-only H_0 value by 3σ . We refer to the corresponding prior as *H073p02*.⁵

A consideration is in order at this point. Given the strong degeneracy between M_ν and H_0 , we expect the introduction of the two aforementioned priors (especially the *H073p02* one) to lead to a tighter bound on M_ν . At the same time, we expect this bound to be less reliable and/or robust. In other words, such a bound would be quite artificial, as it would be driven by a combination of the tension between direct and primary CMB determinations of H_0 and the strong $M_\nu - H_0$ degeneracy. We can therefore expect the fit to degrade when any of the two aforementioned priors is introduced. We nonetheless choose to include these priors for a number of reasons. First, the underlying measurement in Ref. [168] has attracted significant attention, and hence it is worth assessing its impact on bounds on M_ν , subject to the strict caveats we discussed, in light of its potential to break the $M_\nu - H_0$ degeneracy. Next, our results including

⁵We do not include here the latest 3.8% determination of H_0 by the H0LiCOW program. The measurement, based on gravitational time delays of three multiply imaged quasar systems, yields $H_0 = 71.9_{-3.0}^{+2.4} \text{ km s}^{-1} \text{ Mpc}^{-1}$ [169].

the H_0 priors will serve as a warning of the danger of adding data sets which are inconsistent with each other.

E. Optical depth to reionization

The first generation of galaxies ended the dark ages of the Universe. These galaxies emitted UV photons which gradually ionized the neutral hydrogen which had rendered the Universe transparent following the epoch of recombination, in a process known as reionization (see, e.g., Ref. [170] for a review). So far, it is not entirely clear when cosmic reionization took place. Cosmological measurements can constrain the optical depth to reionization τ , which, assuming instantaneous reionization (a very common useful approximation), can be related to the redshift of reionization z_{re} .

Early CMB measurements of τ from WMAP favored an early reionization scenario ($z_{\text{re}} = 10.6 \pm 1.1$ in the instantaneous reionization approximation [171]), requiring the presence of sources of reionization at $z \gtrsim 10$. This result was in tension with observations of Ly- α emitters at $z \approx 7$ (see, e.g., Refs. [172–176]), which suggest that reionization ended by $z \approx 6$. However, the results delivered by the Planck Collaboration in the 2015 public data release, using the large-scale (low- ℓ) polarization observations of the Planck Low Frequency Instrument (LFI) [84] in combination with Planck temperature and lensing data, indicate that $\tau = 0.066 \pm 0.016$ [39], corresponding to a significantly lower value for the redshift of instantaneous reionization, $z_{\text{re}} = 8.8^{+1.2}_{-1.1}$ (see also Ref. [177] for an assessment of the role of the cleaning procedure on the lower estimate of τ and Ref. [178] for an alternative indirect method for measuring large-scale polarization and hence constraining τ using only small-scale and lensing polarization maps), and thus reducing the need for high-redshift sources of reionization [179–183].

The optical depth to reionization is a crucial quantity when considering constraints on the sum of neutrino masses, the reason being that there exist degeneracies between τ and M_ν (see, e.g., Refs. [19,23,30,111,184–186]). If we consider CMB data only (focusing on the TT spectrum), an increase in M_ν , which results in a suppression of structure, reduces the smearing of the damping tail. This effect can be compensated by an increase in τ . Because of the well-known degeneracy between A_s and τ from CMB temperature data (which are sensitive to the combination $A_s e^{-2\tau}$), the value of A_s should also be increased accordingly. However, the value of A_s also determines the overall amplitude of the matter power spectrum, which is furthermore affected by the presence of massive neutrinos, which reduce the small-scale clustering. If, in addition to TT data, low- ℓ polarization measurements are considered, the degeneracy between A_s and τ will be largely alleviated, and, consequently, so will the multiple ones among the A_s , τ , and M_ν cosmological parameters.

Recently, the Planck Collaboration identified, modeled, and removed previously unaccounted for systematic effects

in large angular scale polarization data from the Planck High Frequency Instrument (HFI) [187] (see also Ref. [188]). Using the new HFI low- ℓ polarization likelihood (that has not been made publicly available by the Planck Collaboration), the constraints on τ have been considerably improved, with a current determination of $\tau = 0.055 \pm 0.009$ [187], entirely consistent with the value inferred from the LFI.

In this work, we explore the impact on the constraints on M_ν of adding a prior on τ . Specifically, we impose a Gaussian prior on the optical depth to reionization of $\tau = 0.055 \pm 0.009$, consistent with the results reported in Ref. [187]. We refer to this prior as $\tau 0p055$. We expect this prior to tighten our bounds on M_ν . However, a prior on τ is a proxy for low- ℓ polarization spectra (low- ℓC_ℓ^{EE} , C_ℓ^{BB} , and C_ℓ^{TE}). Therefore, as previously stated, when adding a prior on τ , we remove the low- ℓ polarization data from our data sets, in order to avoid double-counting information, while keeping low- ℓ temperature data.

F. Planck SZ clusters

The evolution with mass and redshift of galaxy clusters offers a unique probe of both the physical matter density, Ω_m , and the present amplitude of density fluctuations, characterized by the root mean squared of the linear overdensity in spheres of radius $8 h^{-1}$ Mpc, σ_8 ; for a review, see, e.g., Ref. [189]. Both quantities are of crucial importance when extracting neutrino mass bounds from large-scale structure, due to the neutrino free-streaming nature.

CMB measurements are able to map galaxy clusters via the SZ effect, which consists of an energy boost to the CMB photons, which are inverse Compton rescattered by hot electrons (see, e.g., Refs. [190–192]). Therefore, the thermal SZ effect imprints a spectral distortion to CMB photons traveling along the cluster line of sight. The distortion consists of an increase in intensity for frequencies higher than 220 GHz and a decrease for lower frequencies.

We shall here make use of cluster counts from the latest Planck SZ clusters catalog, consisting of 439 clusters detected via their SZ signal [89,90]. We refer to the data set as SZ. The cluster counts function is given by the number of clusters of a certain mass M within a redshift range $[z, z + dz]$, i.e., dN/dz :

$$\left. \frac{dN}{dz} \right|_{M > M_{\text{min}}} = f_{\text{sky}} \frac{dV(z)}{dz} \int_{M_{\text{min}}}^{\infty} dM \frac{dn}{dM}(M, z). \quad (18)$$

The dependence on the underlying cosmological model is encoded in the differential volume dV/dz ,

$$\frac{dV(z)}{dz} = \frac{4\pi}{H(z)} \int_0^z dz' \frac{1}{H^2(z')}, \quad (19)$$

through the dependence of the Hubble parameter $H(z)$ on the basic cosmological parameters and further through the dependence of the cluster mass function dn/dM (calculated through N-body simulations) on the parameters Ω_m and σ_8 .

The largest source of uncertainty in the interpretation of cluster counts measurements resides in the masses of clusters themselves, which in turn can be inferred by x-ray mass proxies, relying, however, on the assumption of hydrostatic equilibrium. This assumption can be violated by bulk motion or nonthermal sources of pressure, leading to biases in the derived value of the cluster mass. Further systematics in the x-ray analyses can arise, e.g., due to instrument calibration or the temperature structure in the gas. Therefore, it is clear that determinations of cluster masses carry a significant uncertainty, with a typical $\Delta M/M \sim 10\%$ – 20% , quantified via the cluster mass bias parameter, $1 - b$,

$$M_X = (1 - b)M_{500}, \quad (20)$$

where M_X denotes the x-ray extracted cluster mass and M_{500} denotes the true halo mass, defined as the total mass within a sphere of radius R_{500} , R_{500} being the radius within which the mean overdensity of the cluster is 500 times the critical density at that redshift.

As the cluster mass bias $1 - b$ is crucial in constraining the values of Ω_m and σ_8 , and hence the normalization of the matter power spectrum, it plays an important role when constraining M_ν . We impose a uniform prior on the cluster mass bias in the range $[0.1, 1.3]$, as is done in Ref. [19], in which it is shown that this choice of $1 - b$ leads to the most stringent bounds on the neutrino mass. There exist as well independent lensing measurements of the cluster mass bias, such as those provided by the Weighing the Giants project [193], by the Canadian Cluster Comparison Project [90], and by CMB lensing [194] (see also Ref. [195]). However, we shall not make use of $1 - b$ priors based on these independent measurements, as the resulting value of σ_8 is in slight tension, at the level of $1 - 2\sigma$, with primary CMB measurements (however, see Ref. [196]).

The value of σ_8 indicated by weak lensing measurements is smaller than that derived from CMB-only data sets, favoring therefore quite large values of M_ν , large enough to suppress the small-scale clustering in a significant way. Therefore, we restrict ourselves to the case in which the cluster mass bias is allowed to freely vary between 0.1 and 1.3. It has been shown in Ref. [19] that this choice leads to robust and unbiased neutrino mass limits. In this way, the addition of the *SZ* data set can be considered truly reliable.

IV. RESULTS ON M_ν

We begin here by analyzing the results obtained for the different data sets and their combinations, assessing their robustness. The constraining power of geometrical versus shape large-scale structure data sets will be discussed in Sec. IV A. In Sec. IV B, we apply the method of Ref. [36]

TABLE IV. 95% C.L. upper bounds on the sum of the three active neutrino masses M_ν . The left column lists the combination of cosmological data sets adopted. *PlanckTT* and *lowP* denote measurements of the CMB full temperature and of the low- ℓ polarization anisotropies from the Planck satellite 2015 data release, respectively. $P(k)$ denotes the galaxy power spectrum of the CMASS sample from the SDSS-BOSS data release 12 (DR12), with marginalization over the bias and the shot noise; see Eq. (12). *BAO* refers to the combination of BAO measurements from the BOSS data release 11 LOWZ sample, the 6dFGS survey, and the WiggleZ survey (see Table III). $\tau 0p055$ denotes a prior on the optical depth to reionization of $\tau = 0.055 \pm 0.009$ as measured by the Planck HFI. *H073p02* and *H070p6* denote priors on the Hubble parameter of $H_0 = 73.02 \pm 1.79 \text{ km s}^{-1} \text{ Mpc}^{-1}$ and $H_0 = 70.6 \pm 3.3 \text{ km s}^{-1} \text{ Mpc}^{-1}$, respectively, based on two different HST data analyses. *SZ* consists of Planck cluster counts measurements via thermal Sunyaev-Zeldovich effects. The right column shows the results (95% C.L. upper bounds on M_ν) obtained assuming a degenerate (3 deg) mass spectrum.

Data set	M_ν (95% C.L.)
<i>base</i> \equiv <i>PlanckTT</i> + <i>lowP</i>	<0.716 eV
<i>base</i> + $P(k)$	<0.299 eV
<i>basePK</i> \equiv <i>base</i> + $P(k)$ + <i>BAO</i>	<0.246 eV
<i>basePK</i> + $\tau 0p055$	<0.205 eV
<i>basePK</i> + <i>SZ</i>	<0.239 eV
<i>basePK</i> + <i>H073p02</i>	<0.164 eV
<i>basePK</i> + <i>H070p6</i>	<0.219 eV
<i>basePK</i> + <i>H073p02</i> + $\tau 0p055$	<0.140 eV
<i>basePK</i> + <i>H073p02</i> + $\tau 0p055$ + <i>SZ</i>	<0.136 eV

that is described in Sec. II B to quantify the exclusion limits on the inverted hierarchy given the bounds on M_ν presented in the following. The 95% C.L. upper bounds on M_ν we obtain are summarized in Tables IV, V, VI, and VII. The C.L.s at which our most constraining data sets disfavor the inverted hierarchy, CL_{IH} , obtained through our analysis in Sec. IV B, are reported in Table VIII.

Table IV shows the results for the more conservative approach when considering CMB data, namely, by neglecting high- ℓ polarization data. The limits obtained when the *base* data set is considered are very close to those quoted in

TABLE V. As Table IV, but with the addition of *highP*, referring to the small-scale CMB polarization anisotropies data.

Data set	M_ν (95% C.L.)
<i>basepol</i> \equiv <i>PlanckTT</i> + <i>lowP</i> + <i>highP</i>	<0.485 eV
<i>basepol</i> + $P(k)$	<0.275 eV
<i>basepolPK</i> \equiv <i>basepol</i> + $P(k)$ + <i>BAO</i>	<0.215 eV
<i>basepolPK</i> + $\tau 0p055$	<0.177 eV
<i>basepolPK</i> + <i>SZ</i>	<0.208 eV
<i>basepolPK</i> + <i>H073p02</i>	<0.132 eV
<i>basepolPK</i> + <i>H070p6</i>	<0.196 eV
<i>basepolPK</i> + <i>H073p02</i> + $\tau 0p055$	<0.109 eV
<i>basepolPK</i> + <i>H073p02</i> + $\tau 0p055$ + <i>SZ</i>	<0.117 eV

TABLE VI. As Table IV, but with the $P(k)$ and the BAO data sets replaced by the *BAOFULL* data set, which comprises BAO measurements from the BOSS data release 11 (both CMASS and LOWZ samples), the 6dFGS survey, and the WiggleZ survey (see Table III). The relative constraining power of the geometric technique versus the shape approach can be inferred by comparing the results of the first, second, third, fourth, and fifth rows to those shown in the third, fourth, sixth, eighth, and ninth rows of Table IV, respectively. The result is that, given our current analyses methods, geometrical information is more powerful than shape information; see also the main text and Fig. 2.

Data set	M_ν (95% C.L.)
<i>baseBAO</i> \equiv <i>PlanckTT</i> + <i>lowP</i> + <i>BAOFULL</i>	<0.186 eV
<i>baseBAO</i> + τ 0p055	<0.151 eV
<i>baseBAO</i> + <i>H073p02</i>	<0.148 eV
<i>baseBAO</i> + <i>H073p02</i> + τ 0p055	<0.115 eV
<i>baseBAO</i> + <i>H073p02</i> + τ 0p055 + <i>SZ</i>	<0.114 eV

TABLE VII. As Table VI, but with the addition of *highP*, referring to the small-scale CMB polarization anisotropies data. The relative constraining power of the geometric technique versus the shape approach can be inferred by comparing the results of the first, second, third, fourth, and fifth rows to those shown in the third, fourth, sixth, eighth, and ninth rows of Table V, respectively. The result is that, given our current analyses methods, geometrical information is more powerful than shape information; see also the main text and Fig. 3.

Data set	M_ν (95% C.L.)
<i>basepolBAO</i> \equiv <i>PlanckTT</i> + <i>lowP</i> + <i>highP</i> + <i>BAOFULL</i>	<0.153 eV
<i>basepolBAO</i> + τ 0p055	<0.118 eV
<i>basepolBAO</i> + <i>H073p02</i>	<0.113 eV
<i>basepolBAO</i> + <i>H073p02</i> + τ 0p055	<0.094 eV
<i>basepolBAO</i> + <i>H073p02</i> + τ 0p055 + <i>SZ</i>	<0.093 eV

TABLE VIII. Exclusion C.L.s of the inverted hierarchy from our most constraining data set combinations, obtained through a rigorous model comparison analysis. Only data set combinations which disfavor the IH at >70% C.L. are reported. The first column lists the combination of cosmological data sets adopted; see Table II for definitions. The second column reports the 95% C.L. upper limit on M_ν , obtained assuming the 3 deg spectrum of three massive degenerate neutrinos. The third column reports CL_{IH} , the C.L. at which the IH is disfavored, calculated via Eq. (7). Finally, the last column shows the relative posterior odds for NH versus IH, with the posterior probabilities for both mass orderings obtained via Eq. (6).

Data set	M_ν (95% C.L., 3 deg)	CL_{IH}	P_N/P_I
<i>basepolPK</i> + <i>H073p02</i> + τ 0p055	<0.109 eV	74%	2.8:1
<i>basepolPK</i> + <i>H073p02</i> + τ 0p055 + <i>SZ</i>	<0.117 eV	71%	2.4:1
<i>baseBAO</i> + <i>H073p02</i> + τ 0p055	<0.115 eV	72%	2.6:1
<i>baseBAO</i> + <i>H073p02</i> + τ 0p055 + <i>SZ</i>	<0.114 eV	72%	2.6:1
<i>basepolBAO</i> + τ 0p055	<0.118 eV	71%	2.4:1
<i>basepolBAO</i> + <i>H073p02</i>	<0.113 eV	72%	2.6:1
<i>basepolBAO</i> + <i>H073p02</i> + τ 0p055	<0.094 eV	77%	3.3:1
<i>basepolBAO</i> + <i>H073p02</i> + τ 0p055 + <i>SZ</i>	<0.093 eV	77%	3.3:1

Ref. [19], where a three degenerate neutrino spectrum with a lower prior on M_ν of 0.06 eV was assumed, whereas we have taken a lower prior of 0 eV. Our choice is driven by the goal of obtaining independent bounds on M_ν from cosmology alone, making the least amount of assumptions. This different choice of prior is the reason for the (small) discrepancy in our 95% C.L. upper limit on M_ν (0.716 eV) and the limit found in Ref. [19] (0.754 eV) and, in general, in all the bounds we shall describe in what follows. That is, these discrepancies are due to differences in the volume of the parameter space explored. When $P(k)$ data are added to the *base*, CMB-only data set, the neutrino mass limits are considerably improved, reaching $M_\nu < 0.299$ eV at 95% C.L.

The limits reported in Table IV, while being consistent with those presented in Ref. [23] [obtained with an older BOSS full-shape power spectrum measurement, the DR9 CMASS $P(k)$], are slightly less constraining. We attribute this mild slight loss of constraining power to the fact that the DR12 $P(k)$ appears slightly suppressed on small scales with respect to the DR9 $P(k)$; see Fig. 1. This fact, already noticed for previous data releases, can ultimately be attributed to a very slight change in power following an increase in the mean galaxy density over time due to the tiling (observational) strategy of the survey [197]. The changes are indeed very small, and the broadband shape of the power spectra for different data releases in fact agree very well within error bars. A small suppression in small-scale power, nonetheless, is expected to favor higher values of M_ν , which help explain the observed suppression, and this explains the slight difference between our results and those of Ref. [23].

While the addition of external data sets, such as a prior on τ or Planck SZ cluster counts, leads to mild improvements in the constraints on M_ν , the tightest bounds are obtained when considering the *H073p02* prior on the

Hubble parameter, due to the large existing degeneracy between H_0 and M_ν at the CMB level, and only partly broken via $P(k)$ or BAO measurements. However, as previously discussed, this $H073p02$ measurement shows a significant tension with CMB estimates of the Hubble parameter.⁶ Therefore, the 95% C.L. limits on M_ν of <0.164 , <0.140 , <0.136 eV for the $basePK + H073p02$, $basePK + H073p02 + \tau0p055$ and $basePK + H073p02 + \tau0p055 + SZ$ cases should be regarded as the most aggressive limits one can obtain when considering a prior on H_0 and neglecting high- ℓ polarization data. Indeed, when using the $H070p6$ prior, a less constraining limit of $M_\nu < 0.219$ eV at 95% C.L. is obtained in the $basePK + H070p06$ case, a value that is closer to the limits obtained when additional measurements (not related to H_0 priors) are added to the $basePK$ data combination.

The tension between the $H073p02$ measurement and primary CMB determinations of H_0 implies that the very strong bounds obtained using such a prior are also the least robust and/or reliable. They are almost entirely driven by the aforementioned tension in combination with the strong $M_\nu - H_0$ degeneracy and hence are somewhat artificial. We expect in fact the quality of the fit to deteriorate in the presence of two inconsistent data sets (that is, the CMB spectra and H_0 prior). To quantify the worsening in fit, we compute the $\Delta\chi^2$ associated to the best fit, for a given combination of data sets before and after the addition of the H_0 prior. For example, for the $basePK$ data set combination, we find $\Delta\chi^2 \equiv \chi_{\min}^2(basePK + H073p02) - \chi_{\min}^2(basePK) = +5.2$, confirming as expected a substantial worsening in fit when the $H073p02$ prior is added to the $basePK$ data set. The above observation reinforces the fact that any bound on M_ν obtained using the $H073p02$ prior should be interpreted with considerable caution, as such a bound is most likely artificial.

Table V shows the equivalent to Table IV but including high- ℓ polarization data. Notice that the limits are considerably tightened. As previously discussed, the tightest bounds are obtained when the $H073p02$ prior is considered. For instance, we obtain $M_\nu < 0.109$ eV at 95% C.L. from the $basepolPK + H073p02 + \tau0p055$ data combination. We caution once more against the very tight bounds obtained with the $H073p02$ being most likely artificial. This is confirmed, for example, by the $\Delta\chi_{\min}^2 = +6.4$ between the $basepolPK + H073p02$ and $basepolPK$ data sets.

A. Geometric versus shape information

In the following, we shall compare the constraining power of geometrical probes in the form of BAO measurements versus shape probes in the form of power

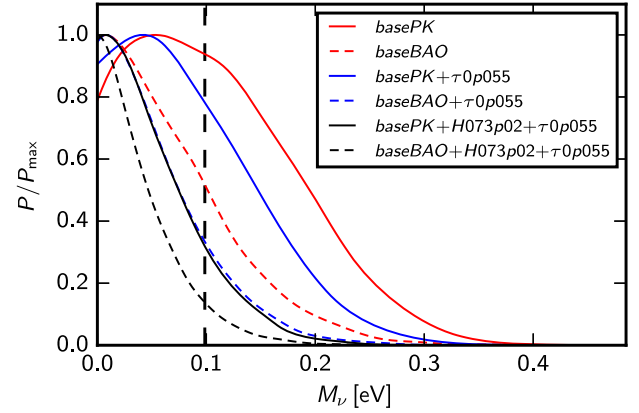


FIG. 2. Posteriors of M_ν obtained with baseline data sets $basePK$ and $baseBAO$, in combination with additional external data sets. This allows for a comparison of the constraining power of shape information in the form of the full-shape galaxy power spectrum and geometrical information in the form of BAO measurements, when CMB full temperature and low- ℓ polarization data are used. To compare the relative constraining power of shape and geometrical information, compare the solid and dashed lines for a given color: red ($basePK$ against $baseBAO$), blue ($basePK + \tau0p055$ against $baseBAO + \tau0p055$), and black ($basePK + H073p02 + \tau0p055$ against $baseBAO + H073p02 + \tau0p055$). The dotted line at $M_\nu = 0.0986$ eV denotes the minimal allowed mass in the IH scenario. It can be clearly seen that with our current analyses methods geometrical information supersedes shape information in constraining power.

spectrum measurements. For that purpose, we shall replace here the DR12 CMASS $P(k)$ and the BAO data sets by the $BAOFULL$ data set, which consists of BAO measurements from the BOSS DR11 (both CMASS and LOWZ samples) survey, the 6dFGS survey, and the WiggleZ survey; see Table III for more details. The main results of this section are summarized in Tables VI and VII as well as Figs. 2 and 3.

Table VI shows the equivalent to the third, fourth, sixth, eighth, and ninth rows of Table IV, but with the shape information from the BOSS DR12 CMASS spectrum replaced by the geometrical BAO information from the BOSS DR11 CMASS measurements. First, we notice that all the geometrical bounds are, in general, much more constraining than the shape bounds, as previously studied and noticed in the literature (see, e.g., Refs. [164,215] and also Refs. [216,217] for recent studies on the subject). These studies have shown that, within the minimal Λ CDM + M_ν scenario, BAO measurements provide tighter constraints on M_ν than data from the full power spectrum shape. Nevertheless, it is very important to assess whether these previous findings still hold with the improved statistics and accuracy of today's large-scale structure data (see the recent Ref. [30] for the expectations from future galaxy surveys).

We confirm that this finding still holds with current data. Therefore, current analyses methods of large-scale structure

⁶See, e.g., Refs. [144,198–214] for recent works examining this discrepancy and possible solutions.

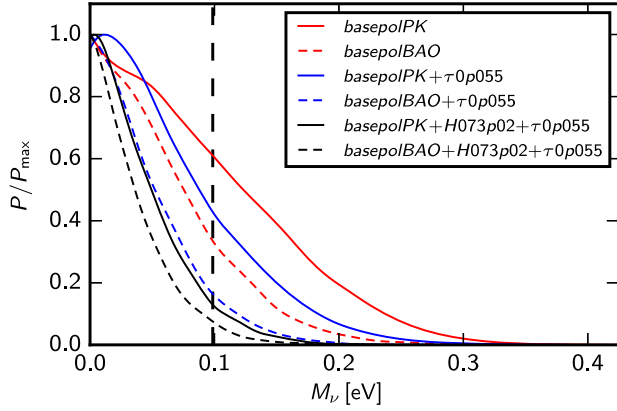


FIG. 3. As Fig. 2, but with the addition of high- ℓ polarization anisotropy data. Hence, the data sets considered are the baseline data sets *basePK* and *baseBAO* and combinations with external data sets. Once more, it can be clearly seen that with our current analyses methods geometrical information supersedes shape information in constraining power.

data sets are such that these are still sensitive to massive neutrinos through background rather than perturbation effects, despite the latter being, in principle, a much more sensitive probe of the effect of massive neutrinos on cosmological observables. However, as we mentioned earlier, this behavior could be reverted once we are able to determine the amplitude and scale dependence of the galaxy bias through CMB lensing, cosmic shear, galaxy clustering measurements, and their cross-correlations (see, e.g., Refs. [128–136]).

Moreover, it is also worth remembering that BAO measurements do include nonlinear information through the reconstruction procedure, whereas the same information is prevented from being used in the power spectrum measurements due to the cutoff we imposed at $k = 0.2 h \text{Mpc}^{-1}$. To fully exploit the constraining power of shape measurements, improvements in our analyses methods are necessary; in particular, it is necessary to improve our understanding of the nonlinear regime of the galaxy power spectrum in the presence of massive neutrinos as well as further our understanding of the galaxy bias at a theoretical and observational level.

The addition of shape measurements requires at least two additional nuisance parameters, which in our case are represented by the bias and shot noise parameters. These two parameters relate the measured galaxy power spectrum to the underlying matter power spectrum, the latter being what one can predict once cosmological parameters are known.⁷ The prescription we adopted relating the galaxy to the matter power spectrum is among the simplest choices.

⁷Moreover, at least another nuisance parameter is required in order to account for systematics in the measured galaxy power spectrum, although the impact of this parameter is almost negligible, as we have checked (see Refs. [23,152,197]).

However, it is not necessarily true that more sophisticated choices with more nuisance parameters would further degrade the constraining power of shape measurements, particularly if we were to obtain a handle on the functional form of the scale-dependent bias [128–136]. On the other hand, it remains true that the possibility of benefiting from a large number of modes by increasing the value of k_{max} (which remains one of the factors limiting the constraining power of shape information compared to geometrical one) would require an exquisite knowledge of nonlinear corrections, a topic which is the subject of many recent investigations, particularly in the scenario in which massive neutrinos are present; see, e.g., Refs. [125,126,218–225]. The conclusion, however, remains that improvements in our current analyses methods, as well as further theoretical and modeling advancements, are necessary to exploit the full constraining power of shape measurements (see also Refs. [226–228]).

Finally, we notice that, even without considering the high- ℓ polarization data, we obtain the very constraining bound of $M_\nu < 0.114 \text{ eV}$ at 95% C.L. for the *baseBAO* + *H073p02* + $\tau 0p055$ + *SZ* data sets. We caution again against the artificialness of bounds obtained using the *H073p02* prior, as the tension with primary CMB determinations in H_0 leads to a degradation in the quality of fit. Nonetheless, even without considering the H_0 prior, we still obtain a very constraining bound of $M_\nu < 0.151 \text{ eV}$ at 95% C.L. In any case, results adopting these data set combinations contribute to reinforcing the previous (weak) cosmological hints favoring the NH scenario [23].

Table VII shows the equivalent to Table VI but with the high- ℓ polarization data set included, i.e., adding the *highP* Planck data set in the analyses. We note that the results are quite impressive, and it is interesting to explore how far one could currently get in pushing the neutrino mass limits by means of the most aggressive and least conservative data sets. The tightest limits we find are $M_\nu < 0.093 \text{ eV}$ at 95% C.L. using the *basepolBAO* + *H073p02* + $\tau 0p055$ + *SZ* data set, well below the minimal mass allowed within the IH. Therefore, within the less conservative approach illustrated here, especially due to the use of the *H073p02* prior, there exists a weak preference from present cosmological data for a normal hierarchical neutrino mass scheme. Neglecting the information from the *H073p02* prior, which leads to an artificially tight bound as previously explained, the preference turns out to be weaker ($M_\nu < 0.118 \text{ eV}$ from the *basepolBAO* + $\tau 0p055$ data set combination) but still present.

We end with a consideration, stemming from the observation that with our current analyses methods BAO measurements are more constraining than full-shape power spectrum ones. This suggests that, despite uncertainties in the modeling of the galaxy power spectrum due to the unknown absolute scale of the latter (in other words, the size of the bias) and nonlinear evolution, the galaxy power

spectrum actually represents a conservative data set given that the bounds on M_ν obtained using the corresponding BAO data set are considerably tighter.

In the remainder of the section, we will be concerned with providing a proper quantification of the statistical significance at which we can disfavor the IH, performing a simple but rigorous model comparison analysis.

B. Exclusion limits on the inverted hierarchy

Here, we apply the method of Ref. [36] that is described in Sec. II B to determine the statistical significance at which the inverted hierarchy is disfavored given the bounds on M_ν just obtained. Our results are summarized in Table VIII. To quantify the exclusion limits on the inverted hierarchy, we apply Eq. (6) to our most constraining data set combinations, where the criterion for choosing these data sets will be explained below.

Note that in Eq. (6) we set $p(N) = p(I) = 0.5$. That is, we assign equal priors to NH and IH, which is not only a reasonable choice when considering only cosmological data sets [36] but is also the most uninformative and most conservative choice when there is no prior knowledge about the hierarchies. In any case, the formalism we adopt would allow us to introduce informative prior information on the two hierarchies, i.e., $p(N) \neq p(I) \neq 0.5$. It would in this way be possible to include information from oscillation experiments, which suggest a weak preference for the normal hierarchy due to matter effects (see, e.g., Refs. [10–14]). Including this weak preference does not significantly affect our results, precisely because the current sensitivity to the neutrino mass hierarchy from both cosmology and oscillation experiments is extremely weak (see also, e.g., Ref. [36]).

We choose to only report the statistical significance at which the IH is discarded for the most constraining data set combinations, that is, those which disfavor the IH at $>70\%$ C.L.; we have checked that the threshold for reaching a $\approx 70\%$ C.L. exclusion limit of the IH is reached by data set combinations which disfavor at 95% C.L. values of M_ν greater than ≈ 0.12 eV. In fact, the most constraining bound within our conservative scheme, obtained through the *baseBAO*+ $\tau 0p055$ combination (thus disfavoring data sets which exhibit some tension with CMB or galaxy clustering measurements, for a 95% C.L. upper limit on M_ν of 0.151 eV), falls short of this threshold and is only able to disfavor the IH at 64% C.L., providing posterior odds for NH versus IH of 1.8:1.

The hierarchy discrimination is improved when small-scale polarization is added to the aforementioned data set combination or when the *H073p02* prior (and eventually SZ cluster counts) are added to the same data set combination, leading to a 71% C.L. and 72% C.L. exclusion of the IH, respectively. Similar levels of statistical significance for the exclusion of the IH are reached when the data set combinations *basepolPK*+*H073p02*+ $\tau 0p055$, *basepolPK*+*H073p02*+ $\tau 0p055$ +*SZ*, and *basepolBAO* + *H073p02*

are considered, leading to 74% C.L., 71% C.L., and 72% C.L. exclusions of the IH, respectively. However, it is worth remembering once more that the latter figures relied on the addition of the *H073p02* prior, which led to less reliable bounds. It is also worth noting that our most constraining data set combination(s), that is, *basepolBAO* + *H073p02* + $\tau 0p055$ (+*SZ*), only provide(s) a 77% C.L. exclusion of the IH.

Our findings are totally consistent with those of Ref. [36] and suggest that an improved sensitivity of cosmological data sets is required in order to robustly disfavor the IH, despite that current data sets are already able to substantially reduce the volume of parameter space available within this mass ordering. In fact, it has been argued in Ref. [36] that a sensitivity of at least ≈ 0.02 eV is required in order to provide a 95% C.L. exclusion of the IH. Incidentally, not only does such a sensitivity seem within the reach of post-2020 experiments [229], but it would also provide a detection of M_ν at a significance of at least 3σ , unless nontrivial late-Universe effects are at play (see, e.g., Refs. [46,47]).

C. Bounds on M_ν in extended parameter spaces: A brief discussion

Thus far, we have explored bounds on M_ν within the assumption of a flat background Λ CDM cosmology. We have used different data set combinations, and have identified the *baseBAO* data set (leading to an upper limit of $M_\nu < 0.186$ eV) combination as being the one providing one of the strongest bounds while at the same time being one of the most robust to systematics and tensions between data sets.

However, we expect the bounds on M_ν would degrade if we were to open the parameter space, that is, if we were to vary additional parameters other than the six base Λ CDM parameters and M_ν . While there is no substantial indication for the need to extend the base set of parameters of the Λ CDM model (see, e.g., Refs. [230,231]), one is nonetheless legitimately brought to wonder about the robustness of the obtained bounds against extended parameter spaces.

While a detailed study belongs to a follow-up paper in progress [232], we nonetheless decide to present two examples of bounds on M_ν within minimally extended parameter spaces. That is, we allow in one case the dark energy equation of state w to vary within the range $[-3, 1]$ (parameter space denoted by Λ CDM + M_ν + w), and in the other case, we allow the curvature energy density Ω_k to vary freely within the range $[-0.3, 0.3]$ (parameter space denoted by Λ CDM + M_ν + Ω_k). Both parameters are known to be relatively strongly degenerate with M_ν , and hence we can expect our allowing them to vary to lead to less stringent bounds on M_ν . In both cases, we consider for simplicity the *baseBAO* data set, for the reasons described above; therefore, the corresponding bound within the Λ CDM + M_ν parameter

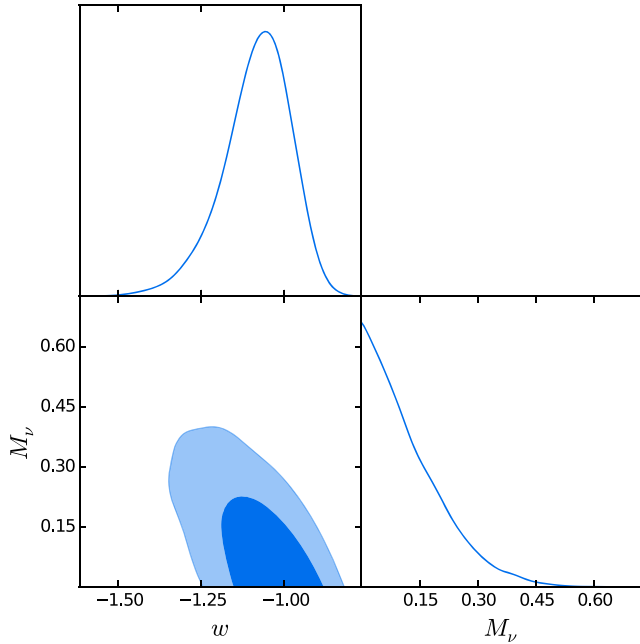


FIG. 4. 68% C.L. (dark blue) and 95% C.L. (light blue) joint posterior distributions in the $M_\nu - w$ plane, along with their marginalized posterior distributions, for the *baseBAO* data combination (see the caption of Table VI for further details). Ticks on the w axis of the upper left plot are the same as those for the lower left plot.

space to which we should compare our results is $M_\nu < 0.186$ eV at 95% C.L., as reported in the first row of Table VI.

For the Λ CDM + $M_\nu + w$ extension, where we leave the dark energy equation of state w free to vary within the range $[-3, 1]$, we can expect the bounds on M_ν to broaden due to a well-known degeneracy between M_ν and w [233]. Specifically, an increase in M_ν can be compensated by a decrease in w , due to the mutual degeneracy with Ω_m . Our results confirm this expectation. With the *baseBAO* data combination, we find $M_\nu < 0.313$ eV at 95% C.L. and $w = -1.08^{+0.09}_{-0.08}$ at 68% C.L., with a correlation coefficient between M_ν and w of -0.56 .⁸ The degeneracy between M_ν and w is clearly visible in the triangle plot of Fig. 4.

For the Λ CDM + $M_\nu + \Omega_k$ extension, where we leave the curvature energy density Ω_k free to vary within the range $[-0.3, 0.3]$, we can again expect the bounds on M_ν to broaden due to the three-parameter geometric degeneracy between h , $\Omega_c h^2$ and Ω_k [111]. For the *baseBAO* data combination, we find $M_\nu < 0.299$ eV at 95% C.L. and $\Omega_k = 0.001^{+0.003}_{-0.004}$ at 68% C.L., with a correlation coefficient between M_ν and Ω_k of 0.60. The degeneracy between M_ν and Ω_k is clearly visible in the triangle plot of Fig. 5.

⁸The correlation coefficient between two parameters i and j (in this case $i = M_\nu$, $j = w$) is defined as $R = C_{ij} / \sqrt{C_{ii}C_{jj}}$, with C the covariance matrix of cosmological parameters.

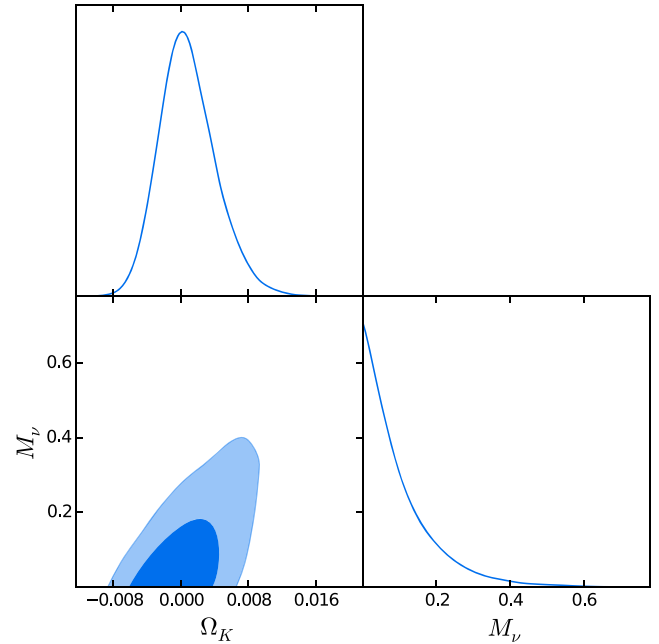


FIG. 5. 68% C.L. (dark blue) and 95% C.L. (light blue) joint posterior distributions in the $M_\nu - \Omega_k$ plane, along with their marginalized posterior distributions, for the *baseBAO* data combination (see the caption of Table VI for further details). Ticks on the Ω_k axis of the upper left plot are the same as those for the lower left plot.

A clarification is in order here: when leaving the dark energy equation of state w and the curvature energy density Ω_k free to vary, it would be extremely useful to add supernovae data, given that these are extremely sensitive to these two quantities. We have, however, chosen not to do so in order to ease comparison with the bound $M_\nu < 0.186$ eV obtained for the same *baseBAO* combination within the Λ CDM + M_ν parameter space. Moreover, in this way, we are able to reach a conservative conclusion concerning the robustness of M_ν bounds to the Λ CDM + $M_\nu + w$ and Λ CDM + $M_\nu + \Omega_k$ parameter spaces, as the addition of supernovae data would lead to tighter bounds than the $M_\nu < 0.313$ eV and $M_\nu < 0.299$ eV quoted.

Of course, as expected, the bounds on M_ν degrade the moment we consider extended parameter spaces. Given our discussion in Sec. IV B, this means within the extended parameter spaces considered the preference for one hierarchy over another essentially vanishes. However, the last statement is not necessarily always true; for instance, in certain models of dynamical dark energy with specific functional forms of $w(z)$, the constraints on M_ν can get tighter. An example is the holographic dark energy model, within which bounds on M_ν have been shown to be substantially tighter than within a Λ CDM Universe [59,63,217]. An interesting thing to note, however, is that within better than 1σ uncertainties (i.e., within $\sim 68\%$ C.L.) both w and Ω_k are compatible with the values to which they are fixed within the minimal Λ CDM + M_ν parameter space, that is, -1 and 0 , respectively.

V. CONCLUSIONS

Neutrino oscillation experiments provide information on the two mass splittings governing the solar and atmospheric neutrino transitions but are unable to measure the total neutrino mass scale, M_ν . The sign of the largest mass splitting, the atmospheric mass gap, remains unknown. The two resulting possibilities are the so-called normal (positive-sign) or inverted (negative-sign) mass hierarchies. While in the normal hierarchy scheme neutrino oscillation results set the minimum allowed total neutrino mass M_ν to be approximately equal to $M_{\nu,\min} \sim 0.06$ eV, in the inverted one, this lower limit is $M_{\nu,\min} \sim 0.1$ eV.

Currently, cosmology provides the tightest bounds on the total neutrino mass M_ν , i.e., on the sum of the three active neutrino states. If these cosmological bounds turned out to be robustly and significantly smaller than the minimum allowed in the inverted hierarchy, then one would indeed determine the neutrino mass hierarchy via cosmological measurements. To prepare ourselves for the hierarchy extraction, an assessment of the cosmological neutrino mass limits, studying their robustness against different priors and assumptions concerning the neutrino mass distribution among the three neutrino mass eigenstates, is mandatory. Moreover, the development and application of rigorous model comparison methods to assess the preference for one hierarchy over the other is necessary. In this work, we have analyzed some of the most recent publicly available data sets to provide updated constraints on the sum of the three active neutrino masses, M_ν , from cosmology.

One very interesting aspect is whether the information concerning the total neutrino mass from the large-scale structure of the Universe in its geometrical form (i.e., via the BAO signature) supersedes that of full-shape measurements of the power spectrum. While previous studies have addressed the question with former galaxy clustering data sets, it is timely to explore the situation with current galaxy catalogs, covering much larger volumes, benefiting from smaller error bars and also from improved, more accurate descriptions of the mildly nonlinear regime in the matter power spectrum.

We find that, despite that the latest measurements of the galaxy power spectrum cover a vast volume of our Universe, the BAO signature extracted from comparable data sets is still more powerful than the full-shape information, within the minimal Λ CDM + M_ν model studied here. This statement is expected to change within the context of extended cosmological models, such as those with nonzero curvature or a time-dependent dark energy equation of state, and we reserve this study for future work [232] (whereas a short discussion on the robustness of the bounds on M_ν within extended parameter spaces is provided in Appendix B).

The reason for the supremacy of BAO measurements over shape information is due to the cutoff in k space imposed when treating the power spectrum. This cutoff is required to avoid the impact of nonlinear evolution. It is

worth remembering once more that BAO measurements contain nonlinear information wrapped in with the reconstruction procedure. This same nonlinear information cannot be used in the power spectrum due to the choice of the conservative cutoff in k space. Moreover, the need for at least two additional nuisance parameters relating the galaxy power spectrum to the underlying matter power spectrum further degrades the constraining power of the latter. Therefore, the stronger constraints obtained through geometrical rather than shape measurements should not be seen as a limitation of the constraining power of the latter but rather as a limitation of methods currently used to analyze these data sets. A deeper understanding of the nonlinear regime of the galaxy power spectrum in the presence of massive neutrinos, as well as further understanding of the galaxy bias at a theoretical and observational level, are required; it is worth noting that a lot of effort is being invested into tackling these issues.

Finally, in this work, we have presented the tightest up-to-date neutrino mass constraints among those which can be found in the literature. Neglecting the debated prior on the Hubble constant of $H_0 = (73.02 \pm 1.79)$ km s⁻¹ Mpc⁻¹, the tightest 95% C.L. upper bound we find is $M_\nu < 0.151$ eV (assuming a degenerate spectrum), from CMB temperature anisotropies, BAO, and τ measurements. Adding Planck high- ℓ polarization data tightens the previous bound to $M_\nu < 0.118$ eV. Further improvements are possible if a prior on the Hubble parameter is also added. In this less conservative approach, the 95% C.L. neutrino mass upper limit is brought down to the level of ~ 0.09 eV, indicating a weak preference for the normal neutrino hierarchy due to volume effects. Our work also suggests that we can identify a restricted set of conservative but robust data sets; this includes CMB temperature data, as well as BAO measurements and galaxy power spectrum data, after adequate corrections for nonlinearities. These data sets allow us to identify a robust upper bound of ~ 0.15 eV on M_ν from cosmological data alone.

In addition to providing updated bounds on the total neutrino mass, we have also performed a simple but robust model comparison analysis, aimed at quantifying the exclusion limits on the inverted hierarchy from current data sets. Our findings indicate that, despite the very stringent upper bounds we have just outlined, current data are not able to conclusively favor the NH over the IH. Within our most conservative scheme, we are able to disfavor the IH with a significance of at most 64% C.L., corresponding to posterior odds of NH over IH of 1.8 : 1. Even the most constraining and less conservative data set combinations are able at most to disfavor the IH at 77% C.L., with posterior odds of NH against IH of 3.3 : 1. This suggests that further improvements in sensitivity, down to the level of 0.02 eV, are required in order for cosmology to conclusively disfavor the IH. Fortunately, it looks like a combination of data from near-future CMB experiments and galaxy surveys should be able to reach this target.

We conclude that our findings, while unable to robustly disfavor the inverted neutrino mass ordering, significantly reduce the volume of parameter space allowed within this mass hierarchy. The more robustly future bounds will be able to disfavor the region of parameter space with $M_\nu > 0.1$ eV, the more the IH will be put under pressure with respect to the NH. In other words future cosmological data, in the absence of a neutrino mass detection, are expected to reinforce the current mild preference for the normal hierarchy mass ordering. On the other hand, if the underlying mass hierarchy is the inverted one, a cosmological detection of the neutrino mass scale could be quickly approaching. In any case, we expect neutrino cosmology to remain an active and exciting field of discovery in the upcoming years.

ACKNOWLEDGMENTS

S. V., E. G., and M. G. acknowledge Hector Gil-Marín for very useful discussions. S. V. and O. M. thank Antonio Cuesta for valuable correspondence. We are very grateful to the anonymous referee for a detailed and constructive report, which enormously helped to improve the quality of our paper. This work is based on observations obtained with Planck (www.esa.int/Planck), an ESA science mission with instruments and contributions directly funded by ESA Member States, NASA, and Canada. We acknowledge use of the Planck Legacy Archive. We also acknowledge the use of computing facilities at NERSC. K. F. acknowledges support from DOE Grant No. DE-SC0007859 at the University of Michigan as well as support from the Michigan Center for Theoretical Physics. M. G., S. V., and K. F. acknowledge support by the Vetenskapsrå det (Swedish Research Council) through Contract No. 638-2013-8993 and the Oskar Klein Centre for Cosmoparticle Physics. M. L. acknowledges support from ASI through ASI/INAF Grant No. 2014-024-R.1 for the Planck LFI Activity of Phase E2. O. M. is supported by PROMETEO II/2014/050, by the Spanish Grant No. FPA2014-57816-P of the MINECO, by MINECO Grant No. SEV-2014-0398, and by the European Union's Horizon 2020 research and innovation programme under the Marie Skłodowska-Curie Grants No. 690575 and No. 674896. O. M. would like to thank the Fermilab Theoretical Physics Department for its hospitality. E. G. is supported by NSF Grant No. AST1412966. S. H. acknowledges support by NASA-EUCLID11-0004, NSF AST1517593, and NSF AST1412966.

APPENDIX A: THE 3 DEG APPROXIMATION

Throughout the paper, we have presented bounds within the 3 deg approximation of a neutrino mass spectrum with three massive degenerate mass eigenstates. The choice was motivated, as discussed in Sec. I, by the observations that the NH and IH mass splittings have a tiny effect on cosmological data, when compared to the 3 deg approximation with the

same value of the total mass M_ν . Here, we discuss the conditions under which this approximation is mathematically speaking valid. We also briefly discuss why the 3 deg approximation is nonetheless physically accurate given the sensitivity of current data.

Mathematically speaking, the 3 deg approximation is valid as long as

$$m_0 \gg |m_i - m_j|, \quad \forall i, j = 1, 2, 3, \quad (\text{A1})$$

where $m_0 = m_1(m_3)$ in the NH (IH) scenario (see Sec. I for the definition of the labeling of the three mass eigenstates). Recall that, according to our convention, $m_1 < m_2 < m_3$ ($m_3 < m_1 < m_2$) in the NH (IH). Therefore, the 3 deg approximation is, strictly speaking, valid when the absolute neutrino mass scale is much larger than the individual mass splittings. A good candidate for a figure of merit to quantify the goodness of the 3 deg approximation can then be obtained by considering the ratio of any given mass difference, over a quantity proportional to the absolute neutrino mass scale. This leads us to consider the figure(s) of merit

$$\zeta_{ij} \equiv \frac{3|m_i - m_j|}{M_\nu}, \quad (\text{A2})$$

where the indices i, j run over $i, j = 1, 2, 3$. The figures of merit ζ_{ij} quantify the goodness of the 3 deg approximation. If the 3 deg approximation were to be exact (which, of course, is physically impossible given the nonzero mass-squared splittings), one would have $\zeta_{ij} = 0$. The 3 deg approximation, then, can be considered valid from a practical point of view as long as ζ_{ij} is sufficiently small, where the amount of deviation from $\zeta_{ij} = 0$ one can tolerate defines what is sufficiently small and hence the validity criterion for the 3 deg approximation.

In Fig. 6, we plot our figure(s) of merit ζ_{ij} , for $i, j = 1, 2$ (red) and $i, j = 1, 3$ (blue) in Eq. (A2) and for the NH (solid) and IH (dashed) scenarios (see the caption for details), against the total neutrino mass M_ν . We plot the same quantities, but this time against the lightest neutrino mass $m_0 = m_1(m_3)$ for the NH (IH), in Fig. 7. As we discussed previously, the 3 deg approximation would be exact if $\zeta_{ij} = 0$ (which of course cannot be displayed due to the choice of a logarithmic scale for the y axis).

As we already discussed, the decision of whether or not 3 deg is a sensible approximation mathematically speaking depends on the amount of deviation from $\zeta_{ij} = 0$ that can be tolerated. As an example, from Figs. 6 and 7, we see that, considering an indicative value of $M_\nu \approx 0.15$ eV, the value of $\zeta_{13} \approx 0.4$, indicating a $\approx 40\%$ deviation from the exact 3 deg scenario, which can hardly be considered small.

This indicates that, within the remaining allowed region of parameter space, the 3 deg approximation is, mathematically speaking, not valid. It is worth remarking that there is a degree of residual model dependency as this

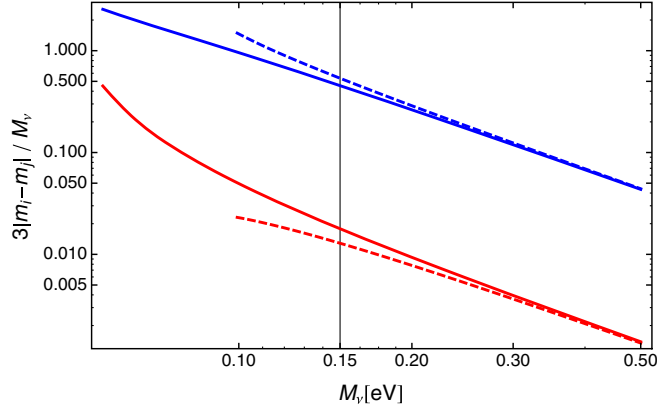


FIG. 6. Figures of merit ζ_{ij} , defined in Eq. (A2) and which quantify the goodness of the 3 deg approximation, as a function of the total neutrino mass M_ν . $\zeta_{ij} = 0$ (not displayed in this plot due to the logarithmic scale on the y axis) corresponds to the unphysical case in which the 3 deg approximation is exact. The red lines correspond to $i, j = 1, 2$ [that is, $\zeta = 3(m_2 - m_1)/M_\nu$], whereas the blue lines correspond to $i, j = 1, 3$ [that is, $\zeta = 3|m_3 - m_1|/M_\nu$], with solid and dashed lines corresponding to the NH and IH scenarios, respectively. The solid vertical line at $M_\nu = 0.15$ eV represents the indicative upper limit on M_ν of 0.15 eV obtained in our analysis.

conclusion was reached taking at face value the indicative upper limit on M_ν of ≈ 0.15 eV, which has been derived under the assumption of a flat Λ CDM background. One can generically expect the bounds we obtained to be loosened to some extent if considering extended cosmological scenarios (although this does not always need to be the case).

A different issue is, instead, whether the 3 deg approximation is physically appropriate, given the sensitivity of current and near-future experiments. The issue has been

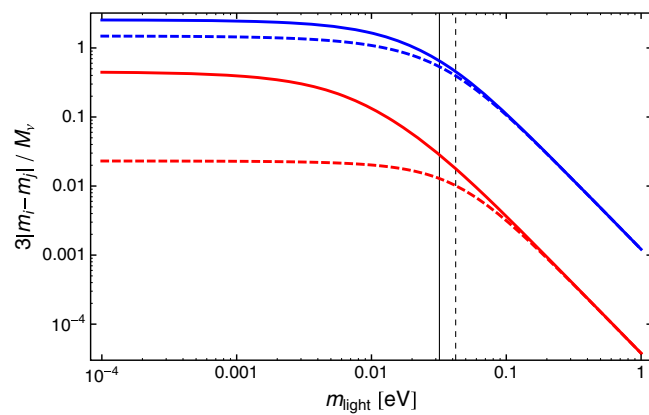


FIG. 7. As Fig. 6, but with the figures of merit plotted against the mass of the lightest mass eigenstate $m_0 = m_1(m_3)$ for NH (IH). The solid and dashed vertical lines at ≈ 0.03 eV and ≈ 0.04 eV, respectively, represent the masses of m_0 corresponding to the indicative upper limit on M_ν of 0.15 eV obtained in our analysis.

discussed extensively in the literature and in particular in some recent works [23,38,112]. It has been argued that, if $M_\nu > 0.1$ eV, future cosmological observations, while measuring M_ν with high accuracy, will not be able to discriminate between the NH and the IH. In any case, cosmological measurements in combination with laboratory experiments will in this case ($M_\nu > 0.1$ eV) play a key role in unraveling the hierarchy [61]. If $M_\nu < 0.1$ eV, most of the discriminatory power in cosmological data between the NH and the IH is essentially due to volume effects, i.e., the fact that oscillation data force $M_{\nu,\min} \approx 0.1$ eV in the IH, implying that the IH has access to a reduced volume of parameter space with respect to the NH.

Another example of the goodness of the 3 deg approximation is provided in Ref. [107], considering a combination of forecasts for CoRE, Euclid, and DESI data. Specifically, Ref. [107] considered a fiducial mock data set generated by implementing the full NH or IH and then studied whether fitting the fiducial data set using the 3 deg approximation rather than the “true” NH or IH would lead to substantial biases. The findings suggest that, apart from small $\mathcal{O}(0.1\sigma)$ reconstruction biases (which can be removed for $M_\nu < 0.1$ eV), the 3 deg approximation is able to recover the fiducial value of M_ν (as long as the free parameter is taken to be consistently either M_ν or m_0). This suggests that, even with near-future cosmological data, the 3 deg approximation will still be sufficiently accurate for the purpose of estimating cosmological parameters and further validates the goodness of the 3 deg approximation in our work.

The conclusion is that current cosmological data sets are sensitive to the total neutrino mass M_ν rather than to the individual masses m_i , implying that the 3 deg approximation is sufficiently precise for the purpose of obtaining reliable cosmological neutrino mass bounds for the time being. On the other hand, for future high-precision cosmological data, which could benefit from increased sensitivity and could reliably have access to nonlinear scales of the matter power spectrum, modeling the mass splittings correctly will matter.

In conclusion, although the 3 deg approximation is not, mathematically speaking, valid in the remaining volume of parameter space, it is, physically speaking, a good approximation given the sensitivity of current data sets. However, quantitative claims about disfavoring the inverted hierarchy have to be drawn with care, making use of rigorous model comparison methods.

APPENDIX B: THE 1 MASS APPROXIMATION

As argued in a number of works, the ability to robustly reach an upper bound on M_ν of ≈ 0.1 eV translates more or less directly into the ability to exclude the inverted hierarchy at a certain statistical significance, as we quantified in Sec. IV B. In this case, it is desirable to check whether one’s conclusions are affected by assumptions on the underlying neutrino mass spectrum. Throughout our

paper, we have presented bounds on M_ν making the assumption of a spectrum of three massive degenerate neutrinos, denoted 3 deg. As we have argued extensively (see, e.g., Appendix A), given the sensitivity of current data, this assumption does not to any significant extent influence the resulting bounds. Nonetheless, it is interesting and timely to investigate the dependence of neutrino mass bounds under assumptions of different mass spectra, which was recently partly done in Ref. [23].

Here, as in Ref. [23], we consider (in addition to the 3 deg spectrum) the approximation spectrum featuring a single massive eigenstate carrying the total mass M_ν together with two massless species. We refer to this scheme by the name “1mass”:

$$m_1 = m_2 = 0, m_3 = M_\nu \quad (1 \text{ mass}). \quad (\text{B1})$$

The motivation for the 1mass choice is twofold: i) it is the usual approximation adopted when performing cosmological analyses with the total neutrino mass fixed to $M_{\nu,\text{min}} = 0.06$ eV, in order to mimic the minimal mass scenario in the case of the NH ($m_1 = 0$ eV, $m_2 \ll m_3$), and ii) it might provide a better description of the underlying neutrino mass ordering in the $M_\nu < 0.1$ eV mass region, in which $m_1 \sim m_2 \ll m_3$, although a complete assessment goes beyond the scope of our work. The latter is the main motivation for exploring the 1mass approximation further, given the recent weak cosmological hints favoring the NH.

Before proceeding, it is useful to clarify why we have chosen to focus on results within the 3 deg scheme. As we discussed, it has been observed that the impact of the NH and IH mass splittings on cosmological data is tiny if one compares the 3 deg approximation to the corresponding NH and IH models with the same value of the total mass M_ν . However, this does not necessarily hold when the comparison is made between 3 deg and 1mass, because the latter always has two pure dark radiation components (see footnote 8 for a definition of dark radiation) throughout the whole expansion history and, in particular, at the present time (on the other hand, NH and IH can have at most one pure radiation component at present time, a situation which occurs in the minimal mass scenario when $m_0 = 0$ eV and thus only for one specific point in neutrino mass parameter space).⁹ The extra massless component(s) present in the 1mass case, but not in the NH and IH (1mass features only one extra component compared to the NH and IH if these

⁹Dark radiation consists of any weakly or noninteracting extra radiation component of the Universe; see, e.g., Ref. [234] for a review and Refs. [235,236] for recent relevant work in connection to neutrino physics. For example, sterile neutrinos may in some models have contributed as dark radiation, see, e.g., Refs. [237,238], or possibly thermally produced cosmological axions [239,240]. Dark radiation might also arise in dark sectors with additional relativistic degrees of freedom which decouple from the Standard Model as, for instance, hidden photons (see, e.g., Refs. [241–252]).

happen to correspond to the minimal mass scenario in which $m_0 = 0$ eV; if $m_0 \neq 0$ eV, 1mass possesses two extra massless components), are known to have a non-negligible impact on cosmological observables, in particular, the CMB anisotropy spectra [23,30].

Let us now discuss how the bounds on M_ν change when passing from the 3 deg to the 1mass approximation. We observe that when considering the *base* data set combinations, and extensions thereof (i.e., the combinations considered in Table IV, in which we report the 3 deg results), the bounds obtained within the 1mass approximation are typically more constraining than the 3 deg ones, by about $\sim 2\%$ – 8% . For example, the 95% C.L. upper bound on M_ν is tightened from 0.716 to 0.658 eV for the *base* combination, from 0.299 to 0.293 eV for the *base + P(k)* combination, and from 0.246 to 0.234 eV for the *basePK* combination. When small-scale polarization data are added (see Table V for the 3 deg results), we observe a reversal in this behavior: that is, the bounds obtained within the 1mass approximation are looser than the 3 deg ones. For example, the 95% C.L. upper bound on M_ν is loosened from 0.485 to 0.619 eV for the *basepol* combination, from 0.275 to 0.300 eV for the *basepol + P(k)* combination, and from 0.215 to 0.228 eV for the *basepolPK* combination.

Regarding the *baseBAO* and *basepolBAO* data set combinations and extensions thereof (see Tables VI and VII for the 3 deg results), no clear trend emerges when passing from the 3 deg to the 1mass approximation, although we note that the bounds typically degrade slightly: for example, the 95% C.L. upper bound on M_ν is loosened from 0.186 to 0.203 eV for the *baseBAO* combination and from 0.153 to 0.155 eV for the *basepolBAO* combination.

We choose not to further investigate the reason behind these tiny but noticeable shifts because, as previously stated, the 1mass distribution is less “physical,” owing to the presence of two unphysical dark radiation states. Instead, we report these numbers in the interest of noticing how these shifts suggest that, at present, cosmological measurements are starting to become sensitive (albeit in a very weak manner) to the late-time hot dark matter versus dark radiation distribution among the neutrino mass eigenstates, a conclusion which had already been reached in Ref. [23].

One of the reasons underlying the choice of studying the 1mass approximation is that this scheme might represent a useful approximation to the minimal mass scenario in the NH. Of course, the possibility that the underlying neutrino hierarchy is inverted is far from being excluded. This raises the question of whether an analogous scheme, which we refer to as “2mass” (already studied in Ref. [23]), might instead approximate the minimal mass scenario in the IH:

$$m_3 = 0, m_1 = m_2 = M_\nu/2 \quad (2 \text{ mass}). \quad (\text{B2})$$

Of course, the previously discussed considerations concerning the nonphysicality of the 1mass approximation (due to the presence of extra pure radiation components)

automatically apply to the 2mass approximation as well. Moreover, we note that bounds on M_ν obtained within the 2 mass approximation (which features one pure radiation state) are always intermediate between those of the 3 deg (which features no pure radiation state) and the 1mass (which features two pure radiation states) ones (see also, e.g., Ref. [23]). This confirms once more that the discrepancy between bounds within these three different approximations is to be attributed to the impact of the unphysical

pure radiation states on cosmological observables, in particular the CMB anisotropy spectra. In conclusion, we remark once more that, while the 3 deg approximation is sufficiently accurate given the precision of current data, other approximations which introduce nonphysical pure radiation states, such as the 1 mass and 2 mass ones, are not. Adopting these to obtain bounds on M_ν might instead lead to unphysical shifts in the determination of cosmological parameters and hence should be avoided.

-
- [1] A. B. McDonald and T. Kajita, Nobel Prize in Physics in 2015, www.nobelprize.org/nobel_prizes/physics/laureates/2015.
- [2] Y. Fukuda *et al.* (Super-Kamiokande Collaboration), *Phys. Rev. Lett.* **81**, 1562 (1998).
- [3] Q. R. Ahmad *et al.* (SNO Collaboration), *Phys. Rev. Lett.* **89**, 011301 (2002).
- [4] T. Araki *et al.* (KamLAND Collaboration), *Phys. Rev. Lett.* **94**, 081801 (2005).
- [5] P. Adamson *et al.* (MINOS Collaboration), *Phys. Rev. Lett.* **101**, 131802 (2008).
- [6] F. P. An *et al.* (Daya Bay Collaboration), *Phys. Rev. Lett.* **108**, 171803 (2012).
- [7] J. K. Ahn *et al.* (RENO Collaboration), *Phys. Rev. Lett.* **108**, 191802 (2012).
- [8] Y. Abe *et al.* (Double Chooz Collaboration), *Phys. Rev. D* **86**, 052008 (2012).
- [9] K. Abe *et al.* (T2K Collaboration), *Phys. Rev. Lett.* **112**, 061802 (2014).
- [10] M. C. Gonzalez-Garcia, M. Maltoni, and T. Schwetz, *J. High Energy Phys.* **11** (2014) 052.
- [11] D. V. Forero, M. Tortola, and J. W. F. Valle, *Phys. Rev. D* **90**, 093006 (2014).
- [12] I. Esteban, M. C. González-García, M. Maltoni, I. Martínez-Soler, and T. Schwetz, *J. High Energy Phys.* **01** (2017) 087.
- [13] F. Capozzi, E. D. Valentino, E. Lisi, A. Marrone, A. Melchiorri, and A. Palazzo, *Phys. Rev. D* **95**, 096014 (2017).
- [14] A. Caldwell, A. Merle, O. Schulz, and M. Totzauer, *Phys. Rev. D* **96**, 073001 (2017).
- [15] F. Capozzi, E. Lisi, A. Marrone, D. Montanino, and A. Palazzo, *Nucl. Phys.* **B908**, 218 (2016).
- [16] E. Giusarma, E. D. Valentino, M. Lattanzi, A. Melchiorri, and O. Mena, *Phys. Rev. D* **90**, 043507 (2014).
- [17] N. Palanque-Delabrouille *et al.*, *J. Cosmol. Astropart. Phys.* **11** (2015) 011.
- [18] E. D. Valentino, E. Giusarma, M. Lattanzi, O. Mena, A. Melchiorri, and J. Silk, *Phys. Lett. B* **752**, 182 (2016).
- [19] E. D. Valentino, E. Giusarma, O. Mena, A. Melchiorri, and J. Silk, *Phys. Rev. D* **93**, 083527 (2016).
- [20] A. J. Cuesta, V. Niro, and L. Verde, *Phys. Dark Universe* **13**, 77 (2016).
- [21] Q. G. Huang, K. Wang, and S. Wang, *Eur. Phys. J. C* **76**, 489 (2016).
- [22] E. D. Valentino, S. Gariazzo, M. Gerbino, E. Giusarma, and O. Mena, *Phys. Rev. D* **93**, 083523 (2016).
- [23] E. Giusarma, M. Gerbino, O. Mena, S. Vagnozzi, S. Ho, and K. Freese, *Phys. Rev. D* **94**, 083522 (2016).
- [24] J. Lesgourgues and S. Pastor, *Phys. Rep.* **429**, 307 (2006).
- [25] Y. Y. Y. Wong, *Annu. Rev. Nucl. Part. Sci.* **61**, 69 (2011).
- [26] J. Lesgourgues and S. Pastor, *Adv. High Energy Phys.* **2012**, 608515 (2012).
- [27] K. N. Abazajian *et al.*, *Astropart. Phys.* **63**, 66 (2015).
- [28] J. Lesgourgues, G. Mangano, G. Miele, and S. Pastor, *Neutrino Cosmology* (Cambridge University Press, Cambridge, England, 2013), p. 378.
- [29] J. Lesgourgues and S. Pastor, *New J. Phys.* **16**, 065002 (2014).
- [30] M. Archidiacono, T. Brinckmann, J. Lesgourgues, and V. Poulin, *J. Cosmol. Astropart. Phys.* **02** (2017) 052.
- [31] J. Lesgourgues, S. Pastor, and L. Perotto, *Phys. Rev. D* **70**, 045016 (2004).
- [32] J. R. Pritchard and E. Pierpaoli, *Phys. Rev. D* **78**, 065009 (2008).
- [33] F. De Bernardis, T. D. Kitching, A. Heavens, and A. Melchiorri, *Phys. Rev. D* **80**, 123509 (2009).
- [34] R. Jiménez, T. Kitching, C. Peña-Garay, and L. Verde, *J. Cosmol. Astropart. Phys.* **05** (2010) 035.
- [35] C. Wagner, L. Verde, and R. Jiménez, *Astrophys. J.* **752**, L31 (2012).
- [36] S. Hannestad and T. Schwetz, *J. Cosmol. Astropart. Phys.* **11** (2016) 035.
- [37] L. Xu and Q. G. Huang, [arXiv:1611.05178](https://arxiv.org/abs/1611.05178).
- [38] M. Gerbino, M. Lattanzi, O. Mena, and K. Freese, *Phys. Lett. B* **775**, 239 (2017).
- [39] P. A. R. Ade *et al.* (Planck Collaboration), *Astron. Astrophys.* **594**, A13 (2016).
- [40] R. Trotta, *Contemp. Phys.* **49**, 71 (2008).
- [41] R. Trotta, [arXiv:1701.01467](https://arxiv.org/abs/1701.01467).
- [42] A. Lewis and S. Bridle, *Phys. Rev. D* **66**, 103511 (2002).
- [43] A. Lewis, *Phys. Rev. D* **87**, 103529 (2013).
- [44] S. Brooks and A. Gelman, *J. Comput. Graph. Stat.* **7**, 434 (1998).
- [45] A. Lewis, post on CosmoCoffee, <http://cosmocoffee.info/viewtopic.php?t=350&sid=adcdc49e35eb4cbf3c69d8273c9980eb>.

- [46] J. F. Beacom, N. F. Bell, and S. Dodelson, *Phys. Rev. Lett.* **93**, 121302 (2004).
- [47] N. Bellomo, E. Bellini, B. Hu, R. Jiménez, C. Peña-Garay, and L. Verde, *J. Cosmol. Astropart. Phys.* **02** (2017) 043.
- [48] S. Joudaki, *Phys. Rev. D* **87**, 083523 (2013).
- [49] M. Archidiacono, E. Giusarma, A. Melchiorri, and O. Mena, *Phys. Rev. D* **86**, 043509 (2012).
- [50] S. M. Feeney, H. V. Peiris, and L. Verde, *J. Cosmol. Astropart. Phys.* **04** (2013) 036.
- [51] M. Archidiacono, N. Fornengo, C. Giunti, S. Hannestad, and A. Melchiorri, *Phys. Rev. D* **87**, 125034 (2013).
- [52] M. Archidiacono, S. Hannestad, A. Mirizzi, G. Raffelt, and Y. Y. Y. Wong, *J. Cosmol. Astropart. Phys.* **10** (2013) 020.
- [53] A. Mirizzi, G. Mangano, N. Saviano, E. Borriello, C. Giunti, G. Miele, and O. Pisanti, *Phys. Lett. B* **726**, 8 (2013).
- [54] L. Verde, S. M. Feeney, D. J. Mortlock, and H. V. Peiris, *J. Cosmol. Astropart. Phys.* **09** (2013) 013.
- [55] S. Gariazzo, C. Giunti, and M. Laveder, *J. High Energy Phys.* **11** (2013) 211.
- [56] M. Archidiacono, N. Fornengo, S. Gariazzo, C. Giunti, S. Hannestad, and M. Laveder, *J. Cosmol. Astropart. Phys.* **06** (2014) 031.
- [57] J. Bergström, M. C. González-García, V. Niro, and J. Salvado, *J. High Energy Phys.* **10** (2014) 104.
- [58] G. Rossi, C. Yèche, N. Palanque-Delabrouille, and J. Lesgourgues, *Phys. Rev. D* **92**, 063505 (2015).
- [59] J. F. Zhang, M. M. Zhao, Y. H. Li, and X. Zhang, *J. Cosmol. Astropart. Phys.* **04** (2015) 038.
- [60] E. D. Valentino, A. Melchiorri, and J. Silk, *Phys. Rev. D* **92**, 121302 (2015).
- [61] M. Gerbino, M. Lattanzi, and A. Melchiorri, *Phys. Rev. D* **93**, 033001 (2016).
- [62] E. D. Valentino, E. Giusarma, M. Lattanzi, O. Mena, A. Melchiorri, and J. Silk, *Phys. Lett. B* **752**, 182 (2016).
- [63] X. Zhang, *Phys. Rev. D* **93**, 083011 (2016).
- [64] T. D. Kitching, L. Verde, A. F. Heavens, and R. Jiménez, *Mon. Not. R. Astron. Soc.* **459**, 971 (2016).
- [65] M. Moresco, R. Jiménez, L. Verde, A. Cimatti, L. Pozzetti, C. Maraston, and D. Thomas, *J. Cosmol. Astropart. Phys.* **12** (2016) 039.
- [66] N. Canac, G. Aslanyan, K. N. Abazajian, R. Easther, and L. C. Price, *J. Cosmol. Astropart. Phys.* **09** (2016) 022.
- [67] M. Archidiacono, S. Gariazzo, C. Giunti, S. Hannestad, R. Hansen, M. Laveder, and T. Tram, *J. Cosmol. Astropart. Phys.* **08** (2016) 067.
- [68] S. Kumar and R. C. Nunes, *Phys. Rev. D* **94**, 123511 (2016).
- [69] E. D. Valentino and F. R. Bouchet, *J. Cosmol. Astropart. Phys.* **10** (2016) 011.
- [70] S. Kumar and R. C. Nunes, *Phys. Rev. D* **96**, 103511 (2017).
- [71] R. Y. Guo, Y. H. Li, J. F. Zhang, and X. Zhang, *J. Cosmol. Astropart. Phys.* **05** (2017) 040.
- [72] X. Zhang, *Sci. China Phys. Mech. Astron.* **60**, 060431 (2017).
- [73] E. K. Li, H. Zhang, M. Du, Z. H. Zhou, and L. Xu, [arXiv:1703.01554](https://arxiv.org/abs/1703.01554).
- [74] W. Yang, R. C. Nunes, S. Pan, and D. F. Mota, *Phys. Rev. D* **95**, 103522 (2017).
- [75] L. Feng, J. F. Zhang, and X. Zhang, *Eur. Phys. J. C* **77**, 418 (2017).
- [76] Y. Dirian, *Phys. Rev. D* **96**, 083513 (2017).
- [77] L. Feng, J. F. Zhang, and X. Zhang, [arXiv:1706.06913](https://arxiv.org/abs/1706.06913).
- [78] C. S. Lorenz, E. Calabrese, and D. Alonso, *Phys. Rev. D* **96**, 043510 (2017).
- [79] F. Couchot, S. Henrot-Versill, O. Perdereau, S. Plaszczynski, B. R. d'Orfeuille, M. Spinelli, and M. Tristram, *Astron. Astrophys.* **606**, A104 (2017).
- [80] C. Doux, M. Penna-Lima, S. D. P. Vinenti, J. Trguer, E. Aubourg, and K. Ganga, [arXiv:1706.04583](https://arxiv.org/abs/1706.04583).
- [81] M. Blennow, *J. High Energy Phys.* **01** (2014) 139.
- [82] F. Simpson, R. Jimenez, C. Pena-Garay, and L. Verde, *J. Cosmol. Astropart. Phys.* **06** (2017) 029.
- [83] T. Schwetz, K. Freese, M. Gerbino, E. Giusarma, S. Hannestad, M. Lattanzi, O. Mena, and S. Vagnozzi, [arXiv:1703.04585](https://arxiv.org/abs/1703.04585).
- [84] N. Aghanim *et al.* (Planck Collaboration), *Astron. Astrophys.* **594**, A11 (2016).
- [85] H. Gil-Marín *et al.*, *Mon. Not. R. Astron. Soc.* **460**, 4188 (2016).
- [86] F. Beutler, C. Blake, M. Colless, D. H. Jones, L. S. -Smith, L. Campbell, Q. Parker, W. Saunders, and F. Watson, *Mon. Not. R. Astron. Soc.* **416**, 3017 (2011).
- [87] C. Blake *et al.*, *Mon. Not. R. Astron. Soc.* **418**, 1707 (2011).
- [88] L. Anderson *et al.* (BOSS Collaboration), *Mon. Not. R. Astron. Soc.* **441**, 24 (2014).
- [89] P. A. R. Ade *et al.* (Planck Collaboration), *Astron. Astrophys.* **594**, A27 (2016).
- [90] P. A. R. Ade *et al.* (Planck Collaboration), *Astron. Astrophys.* **594**, A24 (2016).
- [91] A. Lewis and A. Challinor, *Phys. Rep.* **429**, 1 (2006).
- [92] A. C. Hall and A. Challinor, *Mon. Not. R. Astron. Soc.* **425**, 1170 (2012).
- [93] P. A. R. Ade *et al.* (Planck Collaboration), *Astron. Astrophys.* **571**, A16 (2014).
- [94] K. N. Abazajian *et al.*, *Astropart. Phys.* **63**, 66 (2015).
- [95] K. N. Abazajian *et al.*, *Astropart. Phys.* **63**, 55 (2015).
- [96] K. N. Abazajian *et al.* (CMB-S4 Collaboration), [arXiv:1610.02743](https://arxiv.org/abs/1610.02743).
- [97] M. Levi *et al.* (DESI Collaboration), [arXiv:1308.0847](https://arxiv.org/abs/1308.0847).
- [98] A. Aghamousa *et al.* (DESI Collaboration), [arXiv:1611.00036](https://arxiv.org/abs/1611.00036).
- [99] A. Aghamousa *et al.* (DESI Collaboration), [arXiv:1611.00037](https://arxiv.org/abs/1611.00037).
- [100] E. Calabrese *et al.*, *J. Cosmol. Astropart. Phys.* **08** (2014) 010.
- [101] S. W. Henderson *et al.*, *J. Low Temp. Phys.* **184**, 772 (2016).
- [102] B. A. Benson *et al.* (SPT-3G Collaboration), *Proc. SPIE Int. Soc. Opt. Eng.* **9153**, 91531P (2014).
- [103] A. Suzuki *et al.* (POLARBEAR Collaboration), *J. Low Temp. Phys.* **184**, 805 (2016).
- [104] simonsobservatory.org.
- [105] T. Matsumura *et al.*, *J. Low Temp. Phys.* **176**, 733 (2014).
- [106] F. R. Bouchet *et al.* (CORe Collaboration), [arXiv:1102.2181](https://arxiv.org/abs/1102.2181).
- [107] E. D. Valentino *et al.* (CORe Collaboration), [arXiv:1612.00021](https://arxiv.org/abs/1612.00021).
- [108] F. Finelli *et al.* (CORe Collaboration), [arXiv:1612.08270](https://arxiv.org/abs/1612.08270).

- [109] A. Kogut *et al.*, *J. Cosmol. Astropart. Phys.* **07** (2011) 025.
- [110] G. Efstathiou and J. R. Bond, *Mon. Not. R. Astron. Soc.* **304**, 75 (1999).
- [111] C. Howlett, A. Lewis, A. Hall, and A. Challinor, *J. Cosmol. Astropart. Phys.* **04** (2012) 027.
- [112] M. Gerbino, K. Freese, S. Vagnozzi, M. Lattanzi, O. Mena, E. Giusarma, and S. Ho, *Phys. Rev. D* **95**, 043512 (2017).
- [113] R. Adam *et al.* (Planck Collaboration), *Astron. Astrophys.* **594**, A1 (2016).
- [114] E. Calabrese, A. Slosar, A. Melchiorri, G. F. Smoot, and O. Zahn, *Phys. Rev. D* **77**, 123531 (2008).
- [115] E. D. Valentino, A. Melchiorri, and J. Silk, *Phys. Rev. D* **92**, 121302 (2015).
- [116] E. D. Valentino, A. Melchiorri, and J. Silk, *Phys. Rev. D* **93**, 023513 (2016).
- [117] G. E. Addison, Y. Huang, D. J. Watts, C. L. Bennett, M. Halpern, G. Hinshaw, and J. L. Weiland, *Astrophys. J.* **818**, 132 (2016).
- [118] R. Jiménez, C. Peña-Garay, and L. Verde, *Phys. Dark Universe* **15**, 31 (2017).
- [119] N. Kaiser, *Astrophys. J.* **284**, L9 (1984).
- [120] K. Heitmann, M. White, C. Wagner, S. Habib, and D. Higdon, *Astrophys. J.* **715**, 104 (2010).
- [121] K. Heitmann, E. Lawrence, J. Kwan, S. Habib, and D. Higdon, *Astrophys. J.* **780**, 111 (2014).
- [122] J. Kwan, K. Heitmann, S. Habib, N. Padmanabhan, H. Finkel, E. Lawrence, N. Frontiere, and A. Pope, *Astrophys. J.* **810**, 35 (2015).
- [123] S. Alam *et al.* (BOSS Collaboration), *Mon. Not. R. Astron. Soc.* **470**, 2617 (2017).
- [124] A. Lewis, A. Challinor, and A. Lasenby, *Astrophys. J.* **538**, 473 (2000).
- [125] F. Villaescusa-Navarro, F. Marulli, M. Viel, E. Branchini, E. Castorina, E. Sefusatti, and S. Saito, *J. Cosmol. Astropart. Phys.* **03** (2014) 011.
- [126] M. LoVerde, *Phys. Rev. D* **93**, 103526 (2016).
- [127] A. Raccanelli, L. Verde, and F. Villaescusa-Navarro, arXiv:1704.07837.
- [128] E. Gaztañaga, M. Eriksen, M. Crocce, F. Castander, P. Fosalba, P. Martí, R. Miquel, and A. Cabré, *Mon. Not. R. Astron. Soc.* **422**, 2904 (2012).
- [129] N. Hand *et al.*, *Phys. Rev. D* **91**, 062001 (2015).
- [130] F. Bianchini *et al.*, *Astrophys. J.* **802**, 64 (2015).
- [131] A. R. Pullen, S. Alam, S. He, and S. Ho, *Mon. Not. R. Astron. Soc.* **460**, 4098 (2016).
- [132] F. Bianchini *et al.*, *Astrophys. J.* **825**, 24 (2016).
- [133] D. Kirk *et al.* (DES Collaboration), *Mon. Not. R. Astron. Soc.* **459**, 21 (2016).
- [134] A. Pujol *et al.*, *Mon. Not. R. Astron. Soc.* **462**, 35 (2016).
- [135] S. Singh, R. Mandelbaum, and J. R. Brownstein, *Mon. Not. R. Astron. Soc.* **464**, 2120 (2017).
- [136] J. Prat *et al.* (DES Collaboration), arXiv:1609.08167.
- [137] R. Laureijs *et al.* (EUCLID Collaboration), arXiv:1110.3193.
- [138] C. Carbone, L. Verde, Y. Wang, and A. Cimatti, *J. Cosmol. Astropart. Phys.* **03** (2011) 030.
- [139] S. Joudaki and M. Kaplinghat, *Phys. Rev. D* **86**, 023526 (2012).
- [140] C. Carbone, C. Fedeli, L. Moscardini, and A. Cimatti, *J. Cosmol. Astropart. Phys.* **03** (2012) 023.
- [141] J. Hamann, S. Hannestad, and Y. Y. Y. Wong, *J. Cosmol. Astropart. Phys.* **11** (2012) 052.
- [142] T. Basse, O. E. Bjæ Ide, J. Hamann, S. Hannestad, and Y. Y. Y. Wong, *J. Cosmol. Astropart. Phys.* **05** (2014) 021.
- [143] D. Spergel *et al.*, arXiv:1305.5422.
- [144] V. Poulin, P. D. Serpico, and J. Lesgourgues, *J. Cosmol. Astropart. Phys.* **08** (2016) 036.
- [145] D. J. Eisenstein *et al.* (SDSS Collaboration), *Astron. J.* **142**, 72 (2011).
- [146] A. S. Bolton *et al.* (Cutler Group and LP Collaborations), *Astron. J.* **144**, 144 (2012).
- [147] K. S. Dawson *et al.* (BOSS Collaboration), *Astron. J.* **145**, 10 (2013).
- [148] S. Smee *et al.*, *Astron. J.* **146**, 32 (2013).
- [149] S. Alam *et al.* (SDSS-III Collaboration), *Astrophys. J. Suppl. Ser.* **219**, 12 (2015).
- [150] B. Reid *et al.*, *Mon. Not. R. Astron. Soc.* **455**, 1553 (2016).
- [151] H. J. Seo *et al.*, *Astrophys. J.* **761**, 13 (2012).
- [152] E. Giusarma, R. de Putter, S. Ho, and O. Mena, *Phys. Rev. D* **88**, 063515 (2013).
- [153] R. E. Smith, J. A. Peacock, A. Jenkins, S. D. M. White, C. S. Frenk, F. R. Pearce, P. A. Thomas, G. Efstathiou, and H. M. P. Couchman, *Mon. Not. R. Astron. Soc.* **341**, 1311 (2003).
- [154] R. Takahashi, M. Sato, T. Nishimichi, A. Taruya, and M. Oguri, *Astrophys. J.* **761**, 152 (2012).
- [155] S. Bird, M. Viel, and M. G. Haehnelt, *Mon. Not. R. Astron. Soc.* **420**, 2551 (2012).
- [156] S. Cole *et al.* (2dFGRS Collaboration), *Mon. Not. R. Astron. Soc.* **362**, 505 (2005).
- [157] L. Amendola, E. Menegoni, C. Di Porto, M. Corsi, and E. Branchini, *Phys. Rev. D* **95**, 023505 (2017).
- [158] N. Dalal, O. Dore, D. Huterer, and A. Shirokov, *Phys. Rev. D* **77**, 123514 (2008).
- [159] D. J. Eisenstein and W. Hu, *Astrophys. J.* **496**, 605 (1998).
- [160] Z. Hou, R. Keisler, L. Knox, M. Millea, and C. Reichardt, *Phys. Rev. D* **87**, 083008 (2013).
- [161] Z. Hou *et al.*, *Astrophys. J.* **782**, 74 (2014).
- [162] A. J. Ross, L. Samushia, C. Howlett, W. J. Percival, A. Burden, and M. Manera, *Mon. Not. R. Astron. Soc.* **449**, 835 (2015).
- [163] A. Font-Ribera *et al.* (BOSS Collaboration), *J. Cosmol. Astropart. Phys.* **05** (2014) 027.
- [164] E. Giusarma, R. De Putter, and O. Mena, *Phys. Rev. D* **87**, 043515 (2013).
- [165] A. G. Riess, L. Macri, S. Casertano, H. Lampeitl, H. C. Ferguson, A. V. Filippenko, S. W. Jha, W. Li, and R. Chornock, *Astrophys. J.* **730**, 119 (2011); A. G. Riess, L. Macri, S. Casertano, H. Lampeitl, H. C. Ferguson, A. V. Filippenko, S. W. Jha, W. Li, R. Chornock, and J. M. Silverman, *Astrophys. J.* **732**, 129(E) (2011).
- [166] G. Efstathiou, *Mon. Not. R. Astron. Soc.* **440**, 1138 (2014).
- [167] E. M. L. Humphreys, M. J. Reid, J. M. Moran, L. J. Greenhill, and A. L. Argon, *Astrophys. J.* **775**, 13 (2013).
- [168] A. G. Riess *et al.*, *Astrophys. J.* **826**, 56 (2016).

- [169] V. Bonvin *et al.*, *Mon. Not. R. Astron. Soc.* **465**, 4914 (2017).
- [170] R. Barkana and A. Loeb, *Phys. Rep.* **349**, 125 (2001).
- [171] G. Hinshaw *et al.* (WMAP Collaboration), *Astrophys. J. Suppl. Ser.* **208**, 19 (2013).
- [172] D. P. Stark, R. S. Ellis, K. Chiu, M. Ouchi, and A. Bunker, *Mon. Not. R. Astron. Soc.* **408**, 1628 (2010).
- [173] L. Pentericci *et al.*, *Astrophys. J.* **793**, 113 (2014).
- [174] M. A. Schenker, R. S. Ellis, N. P. Konidaris, and D. P. Stark, *Astrophys. J.* **795**, 20 (2014).
- [175] T. Treu, K. B. Schmidt, M. Trenti, L. D. Bradley, and M. Stiavelli, *Astrophys. J.* **775**, L29 (2013).
- [176] V. Tilvi, C. Papovich, S. L. Finkelstein, J. Long, M. Song, M. Dickinson, H. C. Ferguson, A. M. Koekemoer, M. Giavalisco, and B. Mobasher, *Astrophys. J.* **794**, 5 (2014).
- [177] M. Lattanzi, C. Burigana, M. Gerbino, A. Gruppuso, N. Mandolesi, P. Natoli, G. Polenta, L. Salvati, and T. Trombetti, *J. Cosmol. Astropart. Phys.* **02** (2017) 041.
- [178] P. D. Meerburg, J. Meyers, K. M. Smith, and A. van Engelen, *Phys. Rev. D* **95**, 123538 (2017).
- [179] A. Mesinger, A. Aykutaalp, E. Vanzella, L. Pentericci, A. Ferrara, and M. Dijkstra, *Mon. Not. R. Astron. Soc.* **446**, 566 (2015).
- [180] T. R. Choudhury, E. Puchwein, M. G. Haehnelt, and J. S. Bolton, *Mon. Not. R. Astron. Soc.* **452**, 261 (2015).
- [181] B. E. Robertson, R. S. Ellis, S. R. Furlanetto, and J. S. Dunlop, *Astrophys. J.* **802**, L19 (2015).
- [182] R. J. Bouwens, G. D. Illingworth, P. A. Oesch, J. Caruana, B. Holwerda, R. Smit, and S. Wilkins, *Astrophys. J.* **811**, 140 (2015).
- [183] S. Mitra, T. R. Choudhury, and A. Ferrara, *Mon. Not. R. Astron. Soc.* **454**, L76 (2015).
- [184] R. Allison, P. Caucal, E. Calabrese, J. Dunkley, and T. Louis, *Phys. Rev. D* **92**, 123535 (2015).
- [185] A. Liu, J. R. Pritchard, R. Allison, A. R. Parsons, U. Seljak, and B. D. Sherwin, *Phys. Rev. D* **93**, 043013 (2016).
- [186] E. Calabrese, D. Alonso, and J. Dunkley, *Phys. Rev. D* **95**, 063504 (2017).
- [187] N. Aghanim *et al.* (Planck Collaboration), *Astron. Astrophys.* **596**, A107 (2016).
- [188] R. Adam *et al.* (Planck Collaboration), *Astron. Astrophys.* **596**, A108 (2016).
- [189] S. W. Allen, A. E. Evrard, and A. B. Mantz, *Annu. Rev. Astron. Astrophys.* **49**, 409 (2011).
- [190] Y. B. Zeldovich and R. A. Sunyaev, *Astrophys. Space Sci.* **4**, 301 (1969).
- [191] R. A. Sunyaev and Y. B. Zeldovich, *Astrophys. Space Sci.* **7**, 3 (1970).
- [192] R. A. Sunyaev and Y. B. Zeldovich, *Annu. Rev. Astron. Astrophys.* **18**, 537 (1980).
- [193] A. von der Linden *et al.*, *Mon. Not. R. Astron. Soc.* **443**, 1973 (2014).
- [194] J. B. Melin and J. G. Bartlett, *Astron. Astrophys.* **578**, A21 (2015).
- [195] M. Zaldarriaga and U. Seljak, *Phys. Rev. D* **59**, 123507 (1999).
- [196] T. D. Kitching, J. Alsing, A. F. Heavens, R. Jiménez, J. D. McEwen, and L. Verde, *Mon. Not. R. Astron. Soc.* **469**, 2737 (2017).
- [197] A. Cuesta (private communication).
- [198] A. Pourtsidou and T. Tram, *Phys. Rev. D* **94**, 043518 (2016).
- [199] S. Grandis, D. Rapetti, A. Saro, J. J. Mohr, and J. P. Dietrich, *Mon. Not. R. Astron. Soc.* **463**, 1416 (2016).
- [200] E. D. Valentino, A. Melchiorri, and J. Silk, *Phys. Lett. B* **761**, 242 (2016).
- [201] Q. G. Huang and K. Wang, *Eur. Phys. J. C* **76**, 506 (2016).
- [202] B. L'Huillier and A. Shafieloo, *J. Cosmol. Astropart. Phys.* **01** (2017) 015.
- [203] Y. Chen, S. Kumar, and B. Ratra, *Astrophys. J.* **835**, 86 (2017).
- [204] T. Tram, R. Vallance, and V. Vennin, *J. Cosmol. Astropart. Phys.* **01** (2017) 046.
- [205] J. L. Bernal, L. Verde, and A. G. Riess, *J. Cosmol. Astropart. Phys.* **10** (2016) 019.
- [206] V. V. Luković, R. D'Agostino, and N. Vittorio, *Astron. Astrophys.* **595**, A109 (2016).
- [207] P. Ko and Y. Tang, *Phys. Lett. B* **762**, 462 (2016).
- [208] T. Karwal and M. Kamionkowski, *Phys. Rev. D* **94**, 103523 (2016).
- [209] A. E. Romano, arXiv:1609.04081.
- [210] S. Joudaki *et al.*, *Mon. Not. R. Astron. Soc.* **471**, 1259 (2017).
- [211] A. Shafieloo and D. K. Hazra, *J. Cosmol. Astropart. Phys.* **04** (2017) 012.
- [212] W. Cardona, M. Kunz, and V. Pettorino, *J. Cosmol. Astropart. Phys.* **03** (2017) 056.
- [213] S. Bethapudi and S. Desai, *Eur. Phys. J. Plus* **132**, 78 (2017).
- [214] I. Odderskov, S. Hannestad, and J. Brandbyge, *J. Cosmol. Astropart. Phys.* **03** (2017) 022.
- [215] J. Hamann, S. Hannestad, J. Lesgourgues, C. Rampf, and Y. Y. Y. Wong, *J. Cosmol. Astropart. Phys.* **07** (2010) 022.
- [216] M. M. Zhao, Y. H. Li, J. F. Zhang, and X. Zhang, *Mon. Not. R. Astron. Soc.* **469**, 1713 (2017).
- [217] S. Wang, Y. F. Wang, D. M. Xia, and X. Zhang, *Phys. Rev. D* **94**, 083519 (2016).
- [218] J. Brandbyge, S. Hannestad, T. Haugbølle, and Y. Y. Y. Wong, *J. Cosmol. Astropart. Phys.* **09** (2010) 014.
- [219] K. Ichiki and M. Takada, *Phys. Rev. D* **85**, 063521 (2012).
- [220] E. Castorina, E. Sefusatti, R. K. Sheth, F. Villaescusa-Navarro, and M. Viel, *J. Cosmol. Astropart. Phys.* **02** (2014) 049.
- [221] M. Costanzi, F. Villaescusa-Navarro, M. Viel, J. Q. Xia, S. Borgani, E. Castorina, and E. Sefusatti, *J. Cosmol. Astropart. Phys.* **12** (2013) 012.
- [222] E. Castorina, C. Carbone, J. Bel, E. Sefusatti, and K. Dolag, *J. Cosmol. Astropart. Phys.* **07** (2015) 043.
- [223] C. Carbone, M. Petkova, and K. Dolag, *J. Cosmol. Astropart. Phys.* **07** (2016) 034.
- [224] M. Zennaro, J. Bel, F. Villaescusa-Navarro, C. Carbone, E. Sefusatti, and L. Guzzo, *Mon. Not. R. Astron. Soc.* **466**, 3244 (2017).
- [225] L. A. Rizzo, F. Villaescusa-Navarro, P. Monaco, E. Munari, S. Borgani, E. Castorina, and E. Sefusatti, *J. Cosmol. Astropart. Phys.* **01** (2017) 008.
- [226] N. Hand, U. Seljak, F. Beutler, and Z. Vlah, *J. Cosmol. Astropart. Phys.* **10** (2017) 009.
- [227] C. Modi, M. White, and Z. Vlah, *J. Cosmol. Astropart. Phys.* **08** (2017) 009.

- [228] U. Seljak, G. Aslanyan, Y. Feng, and C. Modi, [arXiv:1706.06645](#).
- [229] J. Errard, S. M. Feeney, H. V. Peiris, and A. H. Jaffe, *J. Cosmol. Astropart. Phys.* **03** (2016) 052.
- [230] M. Raveri, *Phys. Rev. D* **93**, 043522 (2016).
- [231] A. Heavens, Y. Fantaye, E. Sellentin, H. Eggers, Z. Hosenie, S. Kroon, and A. Mootooyaloo, *Phys. Rev. Lett.* **119**, 101301 (2017).
- [232] S. Vagnozzi *et al.* (to be published).
- [233] S. Hannestad, *Phys. Rev. Lett.* **95**, 221301 (2005).
- [234] M. Archidiacono, E. Giusarma, S. Hannestad, and O. Mena, *Adv. High Energy Phys.* **2013**, 191047 (2013).
- [235] A. Banerjee, B. Jain, N. Dalal, and J. Shelton, [arXiv:1612.07126](#).
- [236] C. Brust, Y. Cui, and K. Sigurdson, [arXiv:1703.10732](#).
- [237] E. D. Valentino, A. Melchiorri, and O. Mena, *J. Cosmol. Astropart. Phys.* **11** (2013) 018.
- [238] S. B. Roland and B. Shakya, *J. Cosmol. Astropart. Phys.* **05** (2017) 027.
- [239] A. Melchiorri, O. Mena, and A. Slosar, *Phys. Rev. D* **76**, 041303 (2007).
- [240] J. P. Conlon and M. C. D. Marsh, *J. High Energy Phys.* **10** (2013) 214.
- [241] L. Ackerman, M. R. Buckley, S. M. Carroll, and M. Kamionkowski, *Phys. Rev. D* **79**, 023519 (2009).
- [242] D. E. Kaplan, G. Z. Krnjaic, K. R. Rehermann, and C. M. Wells, *J. Cosmol. Astropart. Phys.* **05** (2010) 021.
- [243] J. M. Cline, Z. Liu, and W. Xue, *Phys. Rev. D* **85**, 101302 (2012).
- [244] F. Y. Cyr-Racine and K. Sigurdson, *Phys. Rev. D* **87**, 103515 (2013).
- [245] J. Fan, A. Katz, L. Randall, and M. Reece, *Phys. Dark Universe* **2**, 139 (2013).
- [246] H. Vogel and J. Redondo, *J. Cosmol. Astropart. Phys.* **02** (2014) 029.
- [247] K. Petraki, L. Pearce, and A. Kusenko, *J. Cosmol. Astropart. Phys.* **07** (2014) 039.
- [248] R. Foot and S. Vagnozzi, *Phys. Rev. D* **91**, 023512 (2015).
- [249] R. Foot and S. Vagnozzi, *Phys. Lett. B* **748**, 61 (2015).
- [250] Z. Chacko, Y. Cui, S. Hong, and T. Okui, *Phys. Rev. D* **92**, 055033 (2015).
- [251] R. Foot and S. Vagnozzi, *J. Cosmol. Astropart. Phys.* **07** (2016) 013.
- [252] K. K. Boddy, M. Kaplinghat, A. Kwa, and A. H. G. Peter, *Phys. Rev. D* **94**, 123017 (2016).